國立清華大學生命科學院分子醫學研究所

碩士論文初稿

Institute of Molecular Medicine
College of Life Science
National TsingHua University
Master Thesis

造成肌病變的 αB-水晶體突變蛋白改變與肌間線蛋白形成的中間絲的交互作用

The Myopathy-Causing Mutation in αB-crystallin Alters Its Interaction with Desmin Intermediate Filament

李哲哲

Sci-Che, Lee

指 導 教 授：彭明德博士 (Dr. Ming-Der, Perng)

中華民國 100 年 11 月

Novenber, 2011

Contents

Abstract

Mutations in the small heat shock protein (sHSP) αB-crystallins cause a range of human diseases including dilated cardiomyopathy (DCM), desmin-related myopathy (DRM) and congenital cataracts. DRM was the first discovered associated with desmin mutations which can affect themselves and closely interacted proteins that typically tending to incomplete assembly of desmin and formation of electro-dense granulofilamentous materials. These diseases involve the disruption of the intermediate filament (IF) cytoskeleton and thus identified intermediate filaments as important physiological targets of sHSPs. Recently, a missense mutation Gly154Ser (G154S) in αB-crystallin was reported to be associated with a late-onset distal vacuolar myopathy without cardiac or respiratory dysfunction and cataracts. This mutation affects a highly conserved amino acid residue among the αB-crystallin in mammals and has been identified earlier in patients with isolated cardiomyopathy. In this study, the effects of G154S mutation on αB-crystallin's ability to interact with desmin IFs was investigated in details using a combination of biochemical, molecular and cell biological approaches. Cosedimentation assay showed that the G154S mutation increased the binding of αB-crystallin to assembled desmin IFs. Transmission electron microscopy confirmed that the G154S αB-crystallin particles decorated the assembled desmin filaments. Transient transfection studies revealed that the expression of G154S αB-crystallin did not affect its distribution but accomplishment of slightly decreased of solubility in C2C12 cell fraction study compared to the wild type αB-crystallin. This is in contrast to the R120G mutation reported in desmin-related myopathy, where this mutation affected the solubility of αB-crystallin and promoted its interaction with desmin filament leading to intracellular aggregates formation in transiently transfected cells. When transfected into a range of cell lines, both R120G and G154S αB-crystallin mutants, but not the wild type protein, increased the phosphorylation of αB-crystallin at Ser^{59} site. Taken together, these data suggest that the G154S mutation may be involved in the pathogenesis of myopathy through a mechanism that is different from the R120G mutation found in DRM.

中文摘要

小型熱休克蛋白：αB水晶體蛋白的突變是造成多種疾病的原因，例如：擴張型心肌病變、肌間線蛋白肌病變，以及先天性的白內障。其中，肌間線蛋白肌病變最早被發現其致病因素直接和肌間線蛋白的突變有關，此突變蛋白不僅改變了本身蛋白質的結構更牽連與它有密切結合關係的蛋白質，進而造成電子密度高的顆粒纖維狀物質的形成。此疾病與中間絲蛋白的細胞骨架瓦解有絕對的相關,由此可知小型熱休克蛋白對於中間絲蛋白具有重要的生理意義。小型熱休克蛋白被認為扮演一個伴隨蛋白的角色，可以和不正常折疊的蛋白質結合並避免形成不正常的蛋白質結構，進而讓細胞遠離逆境壓力。一個位於αB水晶體蛋白上的第154個胺基酸上的誤義突變：由甘胺酸突變成絲胺酸，最近被檢驗出此突變和晚發性的末梢液泡肌病變有關，而與一些典型的心肌病變或是呼吸缺陷還有白內障這些疾病無關。此一突變位於哺乳動物高度保留性的αB水晶體蛋白基因序列中，並更早就被發現於一個罹患單純心肌症的病人檢體中。這項研究藉由生物化學以及分子與細胞生物的方式去探討G154S-αB水晶體蛋白對於肌間線蛋白的交互作用的能力是否因為突變而造成改變。共沉降實驗分析顯示出G154S-αB水晶體蛋白增加了與肌間線蛋白結合的能力。利用穿透式電子顯微鏡觀察此兩種蛋白質的交互作用，也的確出現了G154S-αB水晶體蛋白的顆粒蛋白攀附在肌間線蛋白所形成的中間絲纖維上的現象。而在短暫型DNA轉染細胞系統的研究項目中，實驗數據顯示G154S-αB水晶體蛋白並不會因為突變了而影響它在人類乳癌細胞、老鼠肌原母細胞、以及倉鼠腎細胞裡的分佈，但是在C2C12的細胞比起正常的水晶體蛋白會降低了些微的溶解度。R120G-水晶體蛋白被指出同樣也會造成肌間線蛋白肌病變，藉此可對照R120G-水晶體蛋白在短暫型DNA 轉染細胞系統所引起的，明顯地促進與肌間線蛋白的結合能力、蛋白質溶解度的改變，以及導致形成細胞內不正常蛋白堆積物。另一方面，在R120G-水晶體蛋白和G154S-水晶體蛋白的第59號的絲胺酸上都出現了特殊地磷酸化的現象。綜合以上的研究結果，G154S-水晶體蛋白的致病機制可能與導致肌間線蛋白肌病變的R120G-水晶體蛋白不盡相同。

致謝辭

這篇論文的共耗費了我總共兩年多的時間才得以完成,，雖然過程中遇到了不少的挫折，並發現了許多自己的缺點以及不好的壞習慣，但相對的也發覺了自己的優點並善用之。除了自己的努力以外，沒有指導教授、學長姐的耐心指導，以及同儕間的互相鼓勵打氣，這篇聚集了我兩年多實驗數據的論文是無法順利的完成的。

首先必須感謝我的家人對我經濟上的支持。指導教授對於論文上的內容、排版、編排、邏輯思考、以及最後的修改，花了很多心力以及耐心。在我對於實驗數據以及操作儀器技術上和專業知識上有所困擾時，皆能給於我最適時且適當的解答或建議。女友婉辰不離不棄的相陪，在無數個假日或非假日的時間，傾聽我在實驗室大大小小、開心以及不開心、順利且不順利的種種人事物，並給以我最大的支持。初來乍到，菜鳥味十足，什麼事都懵懵懂懂的我，幸虧實驗室裡的博班學姐美旋給于我各方面的協助和意見，讓我能順利的融入實驗室，以及研究生的生活。博後研究的學長乙菘，在實驗上的討論，並借助他的經驗，讓我對於實驗更能駕輕就熟，並省去了許多不必要的錯誤以及麻煩。以及張慧雲老師實驗室、羅中泉老師實驗室的成員，還有其他生科院實驗室的成員，也陪伴了我度過了很多個日子。大家一起吃飯、聊八卦、運動、出遊，皆能有我有所放鬆並大笑的時候，缺乏了這些因素，這些日子將會非常難熬。然而當大家都畢業了以後，都還會抽空回來聚個餐、聊天，這些都是生活中無法缺少的元素。

最後，我只想說，在經過了充電，磨練，以及實踐的過程後，能夠畢業真的是太爽了…

Abbreviation

BCA	Bicinchoninic acid assay
Co-IP	Co-immunoprecipitation
CryAB	αB-crystallin
Des	Desmin
DRM	Desmin-related myopathy
DCM	Dilated cardiomyopathy
DAPI	4', 6-diamidino-2-phenylindole
IFs	Intermediate filaments
MT	Microtubule
MF	Microfilaemnt
MAPs	Microtubule-associated proteins
NF-H	Neurofilament heavy
NF-M	Neurofilament medium
NF-L	Neurofilament light
P	Pellet
RIPA	Radial immnoprecipitaiton assay buffer
S	Supernatant
ULFs	Unit length filaments
WT	Wild type
NT	No transfected cells
SDS-PAGE	Sodium dodecyl sulfate polyacrylamide gel electrophoresis

Chapter 1：Introduction

1.1 Intermediate filaments

Intermediate filaments (IFs), together with microfilaments (MFs) and microtubules (MTs), form an interconnected cytoskeletal network that gives cells their shape, form and function. Interactions among the three cytoskeletal elements regulate the structural organization of the cytoplasm of animal cells. In contrast to MTs and MFs, which are assembled from highly conserved tubulin and actin that have nucleotide-binding and hydrolyzing activity, IFs are made up of fibrous proteins that have no known enzymatic activity. These proteins have a conserved substructure that is necessary for their self-assembly into IFs of ~10 nm diameter, which is intermediate in size between microfilaments and microtubules. They are, however, characterized also by considerable divergence, especially with respect to the amino-acid sequences of their non-α-helical amino- and carboxy-terminal domains [1, 2]. Of all the three cytoskeletal fibers, IFs are the most diverse and are encoded by at least 70 IF genes, making this gene family one of the largest in the human genome [3, 4]. Based on their gene structure and sequence similarity, IFs are classified into five major families with cell-, tissue-, differentiation- and developmental-specific expression patterns (Table 1). Type I and type II are keratins that are expressed in most epithelial cells. Type III contain four different IF proteins. Among these, vimentin is the most wildly expressed in different cell types. Desmin is the major muscle-specific IF proteins. Glial fibrillary acidic protein (GFAP) expresses mainly in astrocytes of central nervous system and peripherin is predominantly expressed in peripheral nervous system. Type IV IF proteins consist of neurofilament triplet proteins and α-internexin that are mainly expressed in neurons of central nervous systems. Whilst types I–IV IF proteins are localized to the cell cytoplasm, the type V proteins contain nuclear lamins that are

important organizers of the nuclear envelope. Although heterogeneous in size and primary structure, IF proteins share a common tripartite domain structure, with the defining feature being a centrally located α-helical domain containing long-range heptad repeats of characteristic seven-residue periodicity in the distribution of hydrophobic residues in the sequence. The central rod domain mediates coiled-coil dimer formation and represents the major driving force sustaining self-assembly [2, 5]. The central α-helical coiled-coil rod is flanked by flexible, highly variable N- and C-termini that lead to exceptional structural diversity among IFs [6]. This diversity provides many opportunities for tailoring IF networks to cell type-specific functions in contrast to the broadly conserved functions of MT and MF. In most vertebrate cells, intermediate filaments form extensive networks within the cytoplasm. These networks extend throughout the cytoplasm radially in all directions from the nucleus to the cell surface where they provide a scaffold to orchestrate the positioning and function of cellular organelles and to coordinate with other cytoskeletal activities. In the periphery, IFs associate with plasma membrane specialized cellular junctions such as desmosomes, hemidesmosomes and focal adhesions. The resulting network integrates and organizes the cytoplasm providing mechanical integrity that is crucially important for tissue function. The most remarkable feature of IFs is that they can easily self-assemble into 10-nm filaments without any cofactors. Recently, IF assembly has been described *in vitro* as a three-phase scenario [7], in which tetramers first associate laterally into unit-length filaments (ULFs) with approximately 16 nm in diameter and 60 nm in length. In the subsequent elongation phase, the ULFs anneal end-to-end to yield loosely packed filaments that are several hundred nm long. In a third phase, the loosely packed filaments undergo an internal reorganization to yield 10-nm intermediate filaments (Fig. 1). Evidently, this radial compaction that propagates throughout the filament represents an essential step in the conversion of assembly intermediates to mature IFs. Cell culture

studies using live cell imaging as well as immunofluorescence staining of fixed cells have shown that some intermediate filament proteins such as vimentin exists in several organizational states, including non-filamentous particles, short filaments and filamentous networks [8, 9]. The form of vimentin within the particles is unknown at present, although it is possible that they contain oligomeric complexes such as dimers, tetramers or ULFs. *In vitro* studies using bacterially expressed and purified IF protein have yet to reveal any particle-like structures during intermediate filament assembly. However, microinjection experiments have shown that at least for vimentin, the recombinantly purified IF protein associates immediately into non-filamentous particles before assembling into longer intermediate filaments [10]. Although IF proteins are very capable of forming 10-nm filaments in vitro, the consequence of not forming a functional filament network in cells is highlighted in a wide range of human genetic diseases caused by deficiency in this network, including skin fragility and epidermolytic disorders, laminopathies, myopathies, astrogliopathies, neuropathies, cataracts and premature aging [11, 12].

1.2 Desmin and DRM

Demonstration that IFs provide mechanical integrity to tissues first came from pioneering studies showing that mutations in keratins K5 and 14 led to epidermal fragility in mice and epidermolysis bullosa simplex (EBS) in humans [13]. Similar mutations have since then been found in other IF family members leading to identification of a plethora of disease phenotypes [11]. One of these IF-based diseases is the DRM, which is caused by mutations in desmin. Desmin is a type III intermediate filament (IF) protein mainly expressed in cardiac, skeletal, and smooth muscle. It is expressed early in embryogenesis, preceding the expression of many other muscle-specific proteins, such as sarcomericactins, and myosins [14-16]. During myogenic differentiation, an extensive rearrangement in myofibre architecture occurs

where desmin adopts a transverse association with accompanying the alignment of Z bands that anchor actin filaments to at the ends of each sarcomere [17]. By interacting with other IF proteins, such as paranemin [18, 19], synemin [20], syncoilin [21], desmuslin [22] and the cytoskeletal linker protein plectin [23, 24], desmin forms a continuous cytoskeletal network that maintains a spatial relationship between the contractile apparatus and other structural elements of the cell, thus providing maintenance of cellular integrity, force transmission, and mechanochemical signaling. Desmin is much more abundant in heart muscle (2% of total protein) than in skeletal muscle (0.35%) and is a major component of Purkinje fibers, the specialized myocardial conduction system that enables the heart to contract in a coordinated fashion [25]. Desmin gene is located on chromosome 2q35 [26], which encompasses nine exons within an 8.4-kb region and encodes 470 amino acids [27]. The gene is highly conserved among vertebrate species. Like other IF proteins, desmin is organized into three domains with a highly conserved α-helical core of 308 amino acid residues flanked by non-helical N- and C-terminal structures [28]. The α-helical core contains a heptad repeat pattern that two polypeptides to form a homopolymeric coiled-coil dimer, the elementary unit of the desmin IF. The heptad repeat periodicity within the helical rod is interrupted in several places, resulting in four consecutive helical segments known as 1A, 1B, 2A, and 2B that are connected by short nonhelical linkers [29]. To date, the number of known disease-causing desmin mutations has reached 45 (Fig. 2). Although most of these mutations are missense and located within the highly conserved rod domain of desmin, some insertional and frame-shift mutations have also been identified. These include three in-frame deletions of between one and seven amino acids, one exon-skipping mutation, and one insertion of a single nucleotide resulting in premature translation termination. Although most of the mutations have been found throughout the entire desmin sequence, no mutations have thus far been identified in

the 2A helical segment. A characteristic disease pathology that typifies DRM is the presence of protein aggregates containing desmin and αB-crystallin [30], a member of the small heat shock protein family.

1.3 The small heat shock proteins and αB-crystallin

The small heat shock proteins (sHSPs) comprise proteins important in cellular stress response and their ability to protect cells against heat shock and their increased expression as part of the heat shock response contribute to their assignments as heat shock proteins. As the molecular weights of the small heat shock protein subunit are usually less than 30 kDa, the term small was incorporated to distinguish them from the other heat shock proteins. Small heat shock proteins are implicated in different cellular processes, such as suppression of protein aggregation, involvement of cytoskeletal dynamics, cellular growth and differentiation. Of the 10 different small heat shock proteins that are currently known in human [31], some are widely expressed in various tissues, whereas others are more restricted. The αB-crystallin protein has a subunit mass of 20 kDa but forms molecular aggregates with a mass of approximately 650 kDa. Although it was originally discovered and classified as a lens protein, αB-crystallin is found in nonlenticular tissues and is abundant in cardiac and skeletal muscle [32]. Functionally, αB-crystallin acts as a chaperone that responds to stressful conditions by binding to unfolded proteins and preventing their denaturation and aggregation [33]. In addition to modulate correct protein folding, αB-crystallin participates in a number of other cellular processes, including compartment targeting, misfolded/unfolded protein degradation [34, 35], redox homeostasis [36] and apoptosis [37-39].

1.4 Interaction of αB-crystallin with cytoskeletal proteins

The cytoskeleton is the internal structure of the cell that makes the diverse cellular functions possible. The cytoskeletal structures are extremely dynamic, undergoing continual flux within the cytoplasm and requiring continual change in the

protein-protein interactions necessary for their function. It is not surprising that cytoskeletal proteins require the attention of protein chaperones, and specifically small heat shock proteins, to the maintenance and control of the cytoskeleton. Importantly, viewing chaperones and the cytoskeleton as a functional units suggests exciting new possibilities that make us to rethink the general perceived role of chaperones as just quality control proteins. In fact recent studies strongly suggest a far greater potential for the small heat shock proteins, in particular αB-crystallin, in attending the needs of the whole cytoskeleton in both healthy and diseased cells but before I explore these in more detail, it is imperative to discuss the interaction of αB-crystallin with each of the cytoskeletal components. After all, it is from this source that the most unequivocal and strongest evidence has emerged that small heat shock proteins are absolutely required the efficient function of the whole cytoskeleton.

1.5 Actin-based microfilaments and microtubules

Previous studies had shown that αB-crystallin stabilizes actin filaments and regulate actin assembly dynamics in a phosphorylation-dependent manner both in vitro [40, 41] and in cultured cells [42]. Suppressing αB-crystallin gene expression using RNAi technology leads to disruption of the actin microfilament network, further supporting an important role of αB-crystallin in the maintenance of microfilament integrity and ultimately cellular survival [43]. Recently, Gosh et al. reported the identification of several actin interactive sequences in αB-crystallin that could potentially promote actin assembly and also inhibit filament disassembly and aggregation in vitro [44]. Whatever the precise binding sites might be, a direct actin-αB-crystallin interaction probably also occurs in vivo and may participate in the regulation of the actin filament assembly. αB-crystallin is not only important in regulating stability and assembly of actin-based MFs, their interactions with tubulin and MTs have also been documented. It has been reported that αB-crystallin interacts with MTs through MT-associated proteins (MAPs),

and this interaction gives MTs resistance to disassembly both in vitro and in unstressed cells [45]. Further studies revealed that the highly conserved αB-crystallin domain is essential to prevent denatured tubulin from aggregation [46]. Protein pin array technology identifies several tubulin interactive sequences on the surface of human αB-crystallin, providing direct experimental evidence that αB-crystallin can selectively stabilize tubulin as a client protein and collectively modulate MT assembly/disassembly through a dynamic mechanism of sHSP subunit exchange [47].

1.6 Intermediate filaments

Initial studies on the lens cytoskeleton led to the discovery that α-crystallins interact with vimentin [48]. Subsequently it has been shown that both αB-crystallin has temperature-dependent interactions with IFs [49-51]. In vitro assembly studies have also shown that αB-crystallin can inhibit IF assembly and in the case of GFAP, inhibition is independent of phosphorylation [48, 51]. The inhibitory effect of αB-crystallin upon vimentin and GFAP assembly provides a direct regulatory mechanism. Co-immunoprecipitation has demonstrated the associations of sHSPs with soluble IF subunits including vimentin and GFAP [48, 51]. Association of sHSPs with IF networks has also been visualized in a range of cell lines with different IF compositions using immunofluorescence microscopy [51, 52]. Previous studies have provided data to show that the main functions of the αB-crystallin-IF interaction are to maintain the individuality of IFs [51], to modulate inter-filament interactions in their networks [53] and to stabilize assembly intermediates [54]. In skeletal myofibrils and cultured cardiomyocytes, αB-crystallin is colocalized specifically with desmin at the Z-bands [55] and recent studies have demonstrated that in muscle, αB-crystallin serves as a chaperone for desmin and other cytoskeletal proteins preventing them from unintended filament entanglement and subsequent aggregation. Whilst αB-crystallin and IF interaction forms functional complex in normal cells, this interaction is also

observed in a range of pathological conditions. For instance, a characteristic disease pathology that links the different causes of DRM is the presence of aggregates of intermediate filaments containing αB-crystallin in the muscle cells of affected individuals [56, 57]. In fact, there are many diseases where aggregates of IFs and αB-crystallin occur. These include a range of neurodegenerative diseases typified by characteristic cytoplasmic inclusions, such as Pick Bodies [58], Lewy bodies [59] and Rosenthal Fibers [60]. Different IF proteins, namely GFAP and neurofilaments are involved. In alcoholic hepatitis, the characteristic Mallory Bodies that are formed comprise keratin filaments associated with αB-crystallin [61]. So in the disease scenario, these aggregates are typically co-associated with αB-crystallin despite the fact that they involve different intermediate filament proteins. This suggests that the association of αB-crystallin with intermediate filament aggregates is independent of the specific intermediate filament protein but is rather a generic response to this pathological rearrangement of intermediate filaments. Whilst these observations establish a clear link between αB-crystallin, intermediate filaments, and the disease-induced aggregation of intermediate filaments [62], the most compelling evidence that confirms the importance of the αB-crystallin-IF interaction comes from the identification of a mutation in αB-crystallin (R120G), which causes IF aggregation and a phenotype that mimics desmin related myopathies [56]. The clear phenocopy produced by mutations in both αB-crystallin [56] and desmin [63] provides the strongest evidence of the functional link between αB-crystallin and IFs.

1.7 Human diseases associated with αB-crystallin mutations

αB-crystallin has received significant attention in recent years because mutations in the gene encoding αB-crystallin have been linked to human diseases including DRM. Most of the currently known αB-crystallin mutations occurred in highly conserved regions and disease phenotypes associated with αB-crystallin mutations are clinically

heterogeneous. The R120G is by far the most studied αB-crystallin mutation, which was identified originally in a multi-generation French family with autosomal dominant DRM and cataracts [56]. The age of disease onset was in the mid-30s and rate of progression was moderate [56, 64]. The R120 residue is located in the highly conserved region shared by other small heat shock proteins. Structural and functional studies indicate that the αB-crystallin mutant had reduced or completely lost chaperone function [65, 66]. This mutation also decreased the ability of αB-crystallin to interact with the closely related lenticular chaperone αA-crystallin, but strongly interacted with wild type αB-crystallin [67], suggesting a mechanism for dominant negative effect. When transfected into muscle cell lines, R120G αB-crystallin forms intracellular aggregates that contain both desmin and αB-crystallin [56, 66]. Transgenic mice expressing R120G mutant show the presence of protein inclusions that are immunopositive for desmin and αB-crystallinin in cardiomyocyte [68], which compromises cardiac muscle function and results in cardiac hypertrophy. Subsequently, three other mutations in the C-terminal extension were reported for αB-crystallin, but in contrast to the R120G mutation, none caused both cataract and myopathy. The first of these was the 450delA mutation that is associated only with cataract and resulted in a 184-residue product where the coding sequence of the C-terminal extension was altered from residue 150 onwards [69]. Two other mutations were then reported that cause myopathies but not cataract. One mutation with a 2-bp deletion (c.464_465CTdel) in the C terminus of αB-crystallin resulting in a truncated protein of 162 amino acids, instead of the normal 175, was present in a patient with myofibrillar myopathy [70].The mutation was predicted to impair the ability of αB-crystallin to inhibit heat-induced protein aggregation of unfolded and denatured proteins, resulting in aberrant accumulation of proteins in muscle fibers. The other mutation with c.451C>T transition resulting in a p.Gln151X substitution was also identified in a patient with myofibrillar

myopathy [70].The mutation results in a truncated protein of 150 amino acids and is predicted to be functionally deficient. Immunoblots under nondenaturing conditions showed that the mutant protein forms lower than normal molecular mass multimeric complexes with the wild type protein and exerts a dominant-negative effect. Subsequently, a missense R157H mutation in αB-crystallin associated with a late onset dilated cardiomyopathy was reported [71]. This mutation, occurring in an evolutionary conserved amino acid residue, reduces the binding of αB-crystallin to the N2B domain of titin/connectin [71].Very recently, a missense mutation G154S was reported to be associated with a late-onset distal vacuolar myopathy without associated cardiomyopathy, respiratory failure and cataracts [72]. This mutation affects a residue in a highly conserved domain of αB-crystallin, but the effect of such a mutation upon αB-crystallin structure and function has not yet been investigated.

1.8 Molecular pathogenesis of DRM

In vitro studies, together with successful development of cell models and transgenic mice have helped to understand critical pathogenic events in DRM. Based on these studies, the pathomechanism that underlies the development of DRM is beginning to emerge.

1.9 In vitro studies

For DRM caused by desmin mutations, recent investigations have focused on the hypothesis that mutations in the desmin gene lead to defective IF assembly and that this results in aggregation of the mutant protein [57]. Accordingly, Bar et al. showed in a series of elegant studies that mutations in the rod domain of desmin give rise to distinct assembly defects: either they arrested the normal *in vitro* assembly process at specific stages [73] or they led to disassembly of irregular precursor structures [74]. Surprisingly, however, many of the mutations allowed filament formation to take place, although these superficially “normal-looking“ filaments had distinct alterations of

filament architecture, including a change in the number of subunits per cross-section as compared to wild-type desmin IFs [75]. These observations underscore the emerging realization that mutations can contribute to disease in ways that go beyond formation of the filament. The situation in myocytes is even more complex because patients heterozygous for the mutant desmin allele express both mutant and wild type proteins in variable proportions in affected muscle. In vitro studies using a coassembly assay showed that filament formation by assembly-deficient mutant desmins can be rescued in some cases by the presence of wild-type desmin [76]. In many cases, however, the mutant protein drives the wild-type protein into non-IF structures [77]. These *in vitro* analyses were corroborated by transient transfection studies, which revealed that assembly-incompetent desmin mutants formed cytoplasmic aggregates, whereas filament-forming mutants assembled into filamentous networks [73, 74]. A potential disease-causing mechanism that is induced by the filament-forming mutants might be that mutations alter the surface-charge patterns that disturb interaction with important cellular binding partners such as αB-crystallin, leading to accelerated breakdown of the desmin IF network and aggregate formation. Alternatively, an alteration in the intrinsic viscoelastic properties of single desmin filaments might cause a failure in the mechanical coordination of the positioning of individual myofibres. Here, detailed binding studies with IF-associated proteins and analyses of biophysical properties at the single-filament level should help to gain more insight.

1.10 Animal models

Although mice lacking desmin develop normally with no overt phenotypic abnormality in early life, they do develop muscle disorders as they age. Phenotypes include progressive muscle weakness and dystrophic alterations with misalignment of myofibrils and the abnormal distribution of mitochondria in both cardiac and skeletal muscle cells [30, 78]. The severe morphological and functional defects observed in

desmin deficient mice demonstrated that desmin plays a critical role in maintaining the organization of the cytoarchitecture and structural integrity of myofibril, myofibre and the whole muscle tissues. In transgenic mice expressing the R173-D179del desmin mutation that is associated with DRM in humans, examination of the myocardium revealed the accumulation of intracellular aggregates containing desmin and other cytoskeletal proteins [79]. Such aggregates are not seen in desmin-knockout mice, supporting the hypothesis that mutant desmin protein acts as a seed for the formation of protein inclusions in patients with DRM. The aggregates appear as electron-dense granulofilamentous structures, which disrupt the continuity and overall organization of the desmin IF network throughout the cell [79]. In transgenic mice carrying the myopathy-causing human L345P mutation, there is a striking abnormality of mitochondrial morphology and Ca^{2+} handling, suggesting that the mutation impairs mitochondrial integrity in muscle cells [80]. DRM has been recapitulated in transgenic mice by cardiac-specific expression of the αB-R120G protein [79]. These mice develop severe cardiomyopathy with early death at 28 weeks in a gene dosage-dependent manner. Subsequent studies have shown that the defective cardiac chaperone perturbs mitochondrial architecture and impairs mitochondrial function [81]. These changes ultimately lead to cardiomyocyte death, dilation, and heart failure [81]. In another study, Rajasekaran et al. [82] showed that increased glucose-6-phosphate dehydrogenase expression is sufficient to cause cardiomyopathy in transgenic mice, which may represent an alternative mechanism underlying αB-R120G-associated cardiomyopathy [82]. Most recently, Andley et al reported the development of R120G αB-crystallin (αB-R120G) knock-in mice [83]. Both heterozygous and homozygous mutant mice developed myopathy. In skeletal muscle, αB-R120G co-aggregated with desmin, became detergent insoluble, and was ubiquitinated. Moreover, cataract severity increased with age and mutant gene dosage.

These data suggest that the cataract and myopathy pathologies in αB-R120G knock-in mice may share common mechanisms, including increased insolubility of αB-crystallin and its co-aggregation of with IF proteins. Although the detailed molecular basis of cataract and DRM development is not fully understood, the αB-R120G knock-in mice provide a useful model for identifying the effects of molecular mechanisms that affect IF aggregation and lead to cataract formation and DRM.

1.11 Eliminating the aggregates

Chaperones assist normal protein folding and, if necessary, enhance ubiquitination and proteasomal degradation of abnormally constructed proteins. Misfolded desmin or αB-crystallin may escape proteolytic breakdown and accumulate in perinuclear electron-dense bodies [84] known as aggresomes [85]. The aggresomes identified in cardiomyocytes of a mouse expressing the αB-R120G are similar to the accumulations of primary toxic oligomers in neurons of patients with neurodegenerative diseases such as Alzheimer disease [86]. Analysis of aggresome composition also suggests that they contain an amyloid oligomer representing a primary toxic species [87]. Toxic aggregates trigger autophagy as a mechanism for clearing the defective proteins from the muscle fiber [88, 89]. Activation of autophagy has been shown in the αB-R120G mouse model of DRM [90, 91]. Autophagy is considered protective in late-onset neurodegenerative disorders such as Huntington disease and other polyglutamine expansion diseases, and it has been suggested that autophagy upregulation may be a potential strategy for the treatment of a wide range of disorders [92, 93]. A similar approach should be considered in future therapies for the treatment of patients with DRM.

Chapter 2：Material and Methods

2.1 Construction of expression plasmids.

The expression plasmid of human wild type (WT) αB-crystallin was constructed as described previously [54]. In brief, total mRNA was isolated from a sample of human soleus muscle using the RNeasy kit (Qiagen) and converted to cDNA by RT-PCR. Full length human αB-crystallin cDNA was amplified from this cDNA using the nucleotides: 5´-AGCCACCATGGACATCGC-3´ and 5´-CTATTTCTTGGGGGCT GCG-3´ as forward and reverse primer, respectively. The PCR product was cloned into the pGEM®-T Easy vector (Promega) and the sequence confirmed against the GenBanky database entry (Accession No. S45630). The R120G αB-crystallin was constructed by two consecutive PCR amplifications [54] using the mutagenic oligonucleotides 5´-TTCCACGGGAAGTACCGGATCCCAGC-3´ and 5´-CCGGTA CTTCCCGTGGAACTCCCTGGAGATGAA-3´, with the desired A → G mutation at nucleotide position 358 as well as a silent mutation at nucleotide position 363. After confirmation of the mutation by DNA sequencing, the R120G αB-crystallin was subcloned into the *Nco*Iand *Eco*RI restriction sites of the bacterial expression vector pET23d (Novagen). For expression in cultured mammalian cells, both WT and R120G αB-crystallin cDNA were subcloned from the pET23d vector to the mammalian expression vector pcDNA3.1(-) (Invitrogen) with using of the *Xba*I and *Eco*RI restriction sites.

2.2 Construction of G154S αB-crystallin by site directed mutagenesis.

G154S mutation was introduced by site directed mutagenesis with use of WT αB-crystallin in pET23d vector as a template. The following mutagenic oligonucleotides that contained the desired G →A mutation at nucleotide position 460 were synthesized (Mission Biotech, Taipei, Taiwan): 5'-GGAAACAGGTCTCTA

GCCCTGAGCG-3' and 5'-GGTGCGCTCAGGGCTAGAGACCTGT-3', where the substituted nucleotides were underlined. For site directed mutation, the PCR was carried out in a 20 μl reaction containing 10 ng of template, 0.5 μM primer pair, 200 μM dNTPs (NEB) and 0.02 unit of Phusion High Fidelity DNA polymerase (Finnzymes). The PCR cycles were initiated at 98℃ for 30 seconds to denature the template DNA, followed by 20 amplification cycles. PCR cycling was carried out using a G Strom thermal cycler (Gene Technologies, Essex, UK). Each amplification cycle consisted of 98℃ for 30 seconds, 55℃ for 1 minute and 72℃ for 3 minutes. The PCR cycles were finished with an extension step at 72℃ for 10 minutes. The PCR products were treated with 5 units of *Dpn*I (NEB) at 37°C for 1 hour. An aliquot of 10 μl PCR reaction product was analyzed by agarose gel electrophoresis. The full-length plasmid DNA was quantified by band density analysis against the 1636-bp band of the DNA ladders (Fermentas). A 2 μl aliquot of above PCR product was transformed into *E. coli* DH5α competent cells by heat shock at 42℃ for 45 seconds. The transformed cells were spread on a Luria-Bertani (LB) agar plate containing 50 g/ml ampicillin and incubated at 37℃ for 16 hours. Four colonies from each plate were amplified and the plasmid DNA was isolated byFavorPrep™ Plasmid DNA Extraction Mini Kit (Favorgen). The mutation was confirmed by DNA sequencing (Mission Biotech, Taipei, Taiwan). For expression in cultured mammalian cells, the G154S αB-crystallin in the pET23d was subcloned into the pcDNA3.1(-) vector (Invitrogen). Briefly, WT αB-crystallin inpcDNA3.1(-) (Invitrogen) and G154S αB-crystallin in pET23d were both digested with *EcoRI* at 37℃ for 15 minutes. After digestion, the pcDNA3.1(-) vector (Invitrogen) was treated with 1μl calf intestinal phosphatase (CIP, NEB) at 37℃ for 45 minutes. After purification by FavorPrep Gel/PCR Kit, the G154S αB-crystallin and pcDNA3.1(-) vector were ligated by T4 DNA ligase at 16℃ overnight.

2.3 Preparation of competent cells.

One single colony of bacteria was picked and grown in 1 ml LB with appropriate antibiotics overnight at 37℃. The saturated culture of bacteria was inoculated into a 100 ml fresh LB and incubated with vigorous shaking for ~2 hours at 37℃. At this stage, bacteria were grown in an active state, which is required for preparing competent cells. The bacteria were pre-chilled on ice and collected by centrifugation at 4,000 rpm for 20 minutes. The bacterial pellets were resuspended in 20 ml of Competent buffer I (100μM KCl, 60μM$CaC1_2$, 50μM KOAc, 15% glycerol, pH 5.8), followed by incubation on ice for 10 minutes. The bacteria was pelleted by the same centrifugation conditions as mentioned above and resuspended in 4 ml Competent buffer II (100μM KCl, 75μM$CaC1_2$, 10μM MOPS, 15% glycerol, pH 6.8). Aliquots of 100 ml bacterial suspension per Eppendorf tube were prepared and stored at -80℃.

2.4 Expression and purification of recombinant αB-crystallin.

The expression constructs of G154S αB-crystallin were transformed into *Escherichia coli* BL21 (DE3) pLysS strain. After transformation, one well-separated colony was picked and grown in LB with appropriate antibiotics overnight at 37℃. A 10-ml test culture was first set up to check protein expression and optimize the induction conditions. For large-scale αB-crystallin expression, 1.6-liter LB supplemented with 50 g/ml ampicillin and 34 g/ml chloroamphenicol was inoculated with a saturated overnight culture at 1:100 dilution. Bacteria were grown at 37℃ with vigorous shaking at 225 rpm. Once the cultures had reached an OD_{600} of 0.5-0.6 (~2 hours), recombinant protein expression was induced by the addition of 1 mM IPTG for 4 hours. Bacteria were harvested by centrifugation at 6,000 rpm for 30 minutes at 4℃ in a JA-10 rotor (Hitachi). The bacterial pellet was resuspended in TEN buffer (50mM Tris-HCl, pH 8.0, 1mM EDTA, 100mM NaCl and 0.2mM phenylmethylsulfonyl fluoride (PMSF) and 1% (v/v) protease inhibitor cocktails (Sigma, St. Lewis, MO)) and homogenized in a 45-ml Dounce homogenizer.

RNase-free DNase (Promega) was added at 10 U/ml to the crude homogenates and incubated at room temperature for 30 minutes. The homogenate was clarified by centrifugation at 18,000 rpm in a JA-20 rotor (Hitachi) for 30 min at 4℃. The resulting supernatant was collected and polyethyleneimine (50%, Sigma) was added to form a 0.06% (v/v) solution. After incubation on ice for 5 min, the mixture was centrifuged at 16,000 rpm for 10 min to pellet the bacterial DNA.

2.5 Purification of G154S αB-crystallin by column chromatography.

The G154S αB-crystallin was purified to homogeneity by column chromatography with use of an AKTA prime Plus System (GE Healthcare).During the purification, protease inhibitor cocktails (1% (v/v), Sigma) and 0.2mM PMSF were included in all buffers to avoid protein degradation. The purification steps were carried out at room temperature unless stated otherwise. After being dialyzed against column buffer A (20mM Tris-HCl, pH 7.4 and 1mM EDTA) at 4℃ overnight, the clear supernatant was loaded onto a TMAE column (2.6×10 cm) pre-equilibrated with the same buffer. The column was washed with 6 column volumes of column buffer A, and proteins were eluted with a linear gradient of 0–1M NaCl in the same buffer over 1 h at a flow rate of 1 ml/min. The αB-crystallin-enriched fractions were pooled and concentrated by Ultrafree-15 concentrators with a 10,000 molecular weight cutoff (Millipore, UK). The protein sample was then dialyzed against column buffer B (20mM Tris-HCl pH 7.4, 100mM NaCl) overnight at 4℃ and further purified by size exclusion chromatography on a Sephacryl S-400 HR gel filtration column (80 × 1.6 cm) pre-equilibrated in column buffer B. Proteins were eluted from the column with the same buffer over 1 hour at a flow rate of 0.5 ml/min. Column fractions were analyzed by SDS-PAGE and those containing purified αB-crystallin were collected, concentrated and stored at -80℃.

2.6 Determination of protein concentration.

Protein concentration was determined by BCA™ Protein Assay Kit (Pierce, UK) according to manufacturer's instructions. Briefly, bovine serum albumin (BSA) standard protein was serial diluted to concentrations of 2 mg/ml, 1.5 mg/ml, 1 mg/ml, 0.75 mg/ml, 0.5 mg/ml and 0.25 mg/ml. 10 µl each of BSA standards and appropriately diluted protein samples were mixed with 100 µl of working solution (Reagent A and B mixed at 50 : 1 ratio) in a ELISA plate. After incubation at 37℃ for 30 minutes, protein concentrations were estimated by measurement of absorbance at a wavelength of 562 nm on a microplate reader (maker).

2.7 Intermediate filament assembly in vitro.

Purified desmin was diluted to 0.3 mg/ml in 6 M urea in a low ionic strength buffer (10mM Tris-HCl, pH 8.0, 5mM EDTA, 1mM EGTA, and 1mM DTT). Desmin samples were dialyzed stepwise against 3 M urea in the same buffer for 4 h and then against the same buffer without urea overnight at 4℃. Filament assembly was completed by dialyzing against assembly buffer (10mM Tris-HCl, pH 7.0, 100mM NaCl, and 1mM DTT) for 12–16 h at room temperature. The efficiency of in vitro assembly was assessed by high-speed sedimentation assay as described previously (Nicholl and Quinlan, 1994). In brief, the assembly mixture was layered onto a 0.85 M sucrose cushion in assembly buffer and was centrifuged at 80,000 x *g* for 30 min at 20℃. In some experiments, assembled filaments were subjected to low speed centrifugation at 3,000 x *g* for 5 minutes in a Bench Top centrifuge (Eppendorf, Hamburg, Germany) to assess the extent of filament–filament interactions. The supernatant and pellet fractions were separated by 12% (w/v) SDS-PAGE and visualized by Coomassie Blue staining. The amount of protein in the supernatant and pellet fractions was analyzed by a luminescent image analyser (IQ350, GE Healthcare) and quantified using the IQTL software (version 7.0, Healthcare).

2.8 Cosedimentation assay.

WT or mutant αB-crystallin was mixed with desmin in low ionic strength buffer at different molar ratios as indicated. Assembly of desmin filaments in the presence or absence of αB-crystallin was initiated by addition of a 20-fold concentrated assembly buffer to give a final concentration of 100mM imidazole-HCl, pH 6.8, 1mM DTT, 0.2 mM PMSF. After incubation for 1 h at 37℃, protein samples were layered onto a 0.85 M sucrose cushion in the assembly buffer and centrifuged at 80,000×g for 30 min at 20℃ in a TLX-100 Bench Top centrifuge (Beckman Coulter) by using a TLS 55 rotor (Beckman Coulter) to pellet assembled desmin filament and associated proteins. To investigate the effect of αB-crystallin mutation upon aggregate formation in vitro, desmin was assembled in the presence of WT or mutant αB-crystallin and subjected to a low-speed centrifugation at 3,000×g for 5 min in a Bench Top centrifuge (5417R; Eppendorf, Hamburg, Germany). The pellet and supernatant fractions were separated by 12% (wt/vol) SDS-PAGE and visualized by Coomassie Blue staining. The amounts of protein in the supernatant and pellet fractions were analyzed by a luminescent image analyser (IQ350, GE Healthcare) and quantified using the IQTL software (version 7.0, GE Healthcare).

2.9 Transmission electron microscopy.

Protein samples diluted in assembly buffer to 0.3 mg/ml and were negatively stained with 1% (w/v) uranyl acetate (Electron Microscopy Sciences, Hatfield, PA). Samples were spread on glow-discharged, carbon-coated copper grids and examined with a Hitachi H-7500 transmission electron microscope (Hitachi High-Technologies Corporation, Japan), with use of an accelerating voltage of 100 kV. Images were acquired at a magnification of 30,000 × on Kodak 4489 film and then were digitized at 1,200×1,200–pixel resolution before being processed further in Adobe Photoshop CSII (Adobe System, San Jose, CA). Measurement of filaments length and diameter was performed on enlarged electron micrographs using the Image J software (National

Institute of Health, USA).

2.10 Cell culture and transient transfection.

Baby hamster kidney (BHK21) fibroblasts, mouse myoblast (C2C12) cells and human breast cancer epithelial (MCF7) cells were grown in high glucose DMEM medium (Sigma) supplemented with 10% (v/v) fetal calf serum (Invitrogen), 100 U/ml penicillin and 0.1 mg/ml of streptomycin (Invitrogen). All cells were maintained at 37℃ in a humidified incubator of 95% (v/v) air and 5% (v/v) CO_2.For transient transfection experiments, pcDNA3 vector (Invitrogen) containing either WT or mutant αB-crystallin in was prepared using PureLink™ HiPure Plasmid Purification Kits (Invitrogen). Cells grown on 13-mm coverslips at a density of 50–60% confluence were transiently transfected with αB-crystallin constructsby GeneJuice® transfection reagent (Novagen) according to manufacturer's protocol. Cells were allowed to recover for 48 h before processing for immunofluorescence microscopy.

2.11 Generation of stable cell lines.

BHK21 or C2C12 cells grown in 10-cm^2 Petri dish to ~50% confluency were transiently transfected with WT or mutant αB-crystallin using the GeneJuice® transfection reagent (Novagen). The pcDNA3.1/Hygro (Invitrogen) containing hygromycin resistant gene was cotransfected with αB-crystallin construct to increase the selection efficiency. Selection of stable cell lines was initiated 48 hours after transfection using 400 g/ml of G418 (Sigma) and 200 g/ml of hygromycin B (Invitrogen). This concentration was selected based on the sensitivity of C2C12 and BHK21 cells to these antibiotics. Fourteen days after selection, colonies were isolated and cultured in 24-well plates and then transferred into 12-well and 6-well plates (Greiner Bio-One Ltd, Gloucestershire, UK) and finally into 10-cm^2 Petri dishes. Stable cell lines were maintained in standard growth medium supplemented with 200 g/ml G418 and 100 g/ml hygromycin B. The expression and distribution of

αB-crystallin in stable cell lines were examined by immunofluorescence microscopy.

2.12 Immunofluorescence microscopy.

Cells grown on coverslip were washed twice with PBS and fixed in either ice-cold methanol/acetone (1:1 (v/v])) for 20 min or in 4% (w/v) paraformaldehyde/PBS for 10 min. In the case of paraformaldehyde fixation, cells were subsequently permeabilized with 0.5% Triton X-100 in PBS for 10 min. After being washed twice with PBS containing 0.02% (w/v) sodium azide and 0.02% (w/v) BSA (PBS/BSA/azide), cells were blocked with 10% (v/v) goat serum in PBS/BSA/azide for 20 minutes. Cells were incubated with primary antibodies at room temperature for 1 h. The following primary antibodies used in this study were mouse monoclonal anti-αB-crystallin (2D2B6, 1:500 (Sawada, Agata et al. 1993)), monoclonal anti-HSP25 (Stresgen), monoclonal anti-HSP70 (W27, Santa Cruz), monoclonal anti-actin (AC-15, Santa Cruz), rabbit polyclonal anti-desmin (1:100) and polyclonal anti-αB-crystallin (Stressgen). After cells were washed with PBS/BSA/azide, the primary antibodies were detected using Alexa 488 (1:600, Invitrogen) or Alexa 594 (1:600, Invitrogen) conjugated secondary antibodies. All antibodies were diluted in PBS/BSA/azide buffer. The glass coverslips were mounted on slides with the fluorescent protecting agent Citifluor (Sigma). Slides were observed with a Zeiss LSM 510 confocal laser scanning microscope (Carl Zeiss) taking 1.0-mm optical sections. Images were collected in multi-track mode and processed for figures with Adobe Photoshop CSII (Adobe Systems, San Jose, CA). Quantification of the αB-crystallin phenotypes was by visual assessment of the cells and by scoring cells for the presence or absence of αB-crystallin-containing aggregates. Approximately 100–150 transfected cells were assessed, and each experiment was repeated at least three times.

2.13 Cellular fractionation.

Cells grown on 10-cm diameter Petri dishes were transfected with control vector

(pcDNA3.1) or the same containing either WT or mutant αB-crystallin. At 48 hours after transfection, cells were lysed using two different extraction buffers, designed to test the effect of mutation on the solubility of αB-crystallin [94]. In the mild extraction protocol, cells were lysed on ice for 10 minutes in Triton extraction buffer (10mM Tris-HCl, pH 7.6, 140mM NaCl, 5mM EDTA, 1mM EGTA, 1% (v/v) Triton X-100, with protease inhibitor cocktails (Sigma, St. Louis, MO) and 1mM PMSF). In the harsh extraction protocol, cells were lysed in radioimmunoprecipitation assay (RIPA) lysis buffer (Triton extraction buffer containing 0.5% (w/v) sodium deoxycholate and 0.1% (w/v) SDS). Cell lysates were then homogenized in a Douncehomogeniser (Wheaton, Millville, NJ). Total cell lysates were prepared by mixing a small aliquot of the cell lysate with an appropriate volume of Laemmli sample buffer. To prepare supernatant and pellet fractions, total cell lysates were centrifuged at 12,000 rpm at 4°C for 10 minutes in a benchtop centrifuge (Eppendorf, Hamburg, Germany). The resulting pellets were resuspended in the pelleting buffer (20mM Tris-HCl, pH 8.0, 10mM $MgCl_2$ and 1mM PMSF) containing 100 U/ml RNase-free DNase (Promega, UK) and were incubated at room temperature for 1 hour. The pellets were then homogenized and were repelleted by centrifugation at 12,000 rpm at 4℃ for 5 minutes. The final pellets were washed in PBS containing 1mM PMSF and resuspended in Laemmli's sample buffer, in a volume that was proportional to the supernatant before being analyzed by SDS-PAGE and immunoblotting.

2.14 Preparation of cytoskeletal fractions.

The IF-enriched cytoskeletal fractions were prepared as described [95]. In brief, confluent cells grown on 10-cm diameter Petri dish were washed with cold PBS several times, followed by incubation with Triton buffer (10mM Tris-HCl, pH 7.4, 140mM NaCl, 1% (w/v) Triton X-100) for 5 minutes at room temperature. After

removal of the Triton buffer, cells were incubated with high salt buffer (10mM Tris-HCl, pH 7.4, 1.5M KCl, 140mM NaCl, 0.5% (w/v) Triton X-100) on ice for 30 minutes. Cells were then collected by a rubber policeman and homogenized in a 15-cm homogenizer (Wheaton, Millville, NJ). The cell homogenates were centrifuged at 4,000 rpm at 4^{O}C for 20 minutes and the resulting pellet was collected, washed with PBS and resuspended in Tris buffer (10mM Tris-HCl, pH 7.4, 140mM NaCl, 5mM EDTA). After being repelleted by centrifugation at 10,000 rpm at 4℃ for 10 minutes in a pre-cooled benchtop centrifuge (Eppendorf, Hamburg, Germany), the final pellet was resuspended in Laemmli's sample buffer before being analyzed further by SDS-PAGE and immunoblotting.

2.15 Immunoprecipitation.

For immunoprecipitation (IP) experiments, cells were trypsinized and collected by centrifugation at 1,000 rpm for 5 minutes. The cell pellet was washed once with PBS and then homogenized on ice in RIPA buffer (10mM Tris-HCl, pH 7.6, 140mM NaCl, 5mM EDTA, 1mM EGTA, 1% (v/v) Triton X-100, 0.5% (w/v) sodium deoxycholate and 0.1% (w/v) SDS, 1% (v/v) protease inhibitor cocktails (Sigma, St. Louis, MO) and 1mM PMSF). The homogenate was centrifuged at 12,000 rpm at 4℃ for 10 minutes and the resulting supernatant was used for subsequent immunoprecipitation. An aliquot of 0.5 ml of the supernatant was incubated with 20 ml of protein G Sepharose (GE Healthcare, Uppsala, Sweden) followed by centrifugation at 2,500 rpm for 3 minutes. The pre-cleared supernatant was incubated with monoclonal anti-αB-crystallin antibody on ice for 2 hours, followed by incubation with 20 μl of protein G Sepharose in an end-over-end rotator at 4℃ overnight. The immunoprecipitate was collected by centrifugation at 2,500 rpm at 4℃ for 3 minutes. After being washed with RIPA buffer without SDS four times, the immunocomplex was pelleted and resuspended in Laemmli's sample buffer prior to SDS-PAGE and

immunoblotting analysis.

2.16 Immunoblotting.

Immunoblotting was performed using the semi-dry blotting method according to the manufacturer's specifications (Bio-Rad Laboratories, UK). After blotting, protein transfer efficiency was assessed by Ponceau S (Sigma, St. Louis, MO) staining of the nitrocellulose membrane followed by destaining in Tris-buffered saline (TBS, 20mM Tris-HCl, pH 7.4 and 150mM NaCl). Membranes were blocked for 1 hour in blocking buffer containing (3% (w/v) bovine serum albumin in TBS containing 0.1% (v/v) Tween 20 (TTBS) and incubated for 1 hour with primary antibodies at room temperature. The following primary antibodies used in this study were mouse monoclonal anti-desmin (1:2500, D33, DakoCytomation), polyclonal anti-desmin (1:2500), monoclonal anti-HSP27 (G3.1, 1:2500, Abcam, Cambridge MA), monoclonal anti-αB-crystallin (2D2B6, 1:2500, [96]), monoclonal anti-HSP70 (1:2500), monoclonal anti-actin (1:2500, AC-40, Sigma, St. Louis, MO), In some experiments, the membrane was probed with rabbit polyclonal anti-[pSer^{59}] αB-crystallin (1:1000, Enzo), polyclonal anti-HSP25 (1:1000), monoclonal anti-caspase 3 (1:1000, Cell Signaling Technology, Danvers, MA) antibodies diluted by 1:1,000 in blocking buffer. After several washes with TTBS, the membrane was incubated for 1 hour with horseradish peroxidase (HRP)-conjugated secondary antibodies (Dako Cytomation) diluted by 1:2,000 in blocking buffer, followed by washing with TBS for 30 minutes with several changes. Antibody labeling was detected by enhanced chemiluminescence (Western Lightning Plus-ECL, Perkin Elmer) with use of a luminescent image analyser (Image Quant 350, GE Healthcare, Uppsala, Sweden). The strength of signal was quantified using the image analysis software (Image Quant TL 7.0, GE Healthcare, Uppsala, Sweden).

2.17 Silver staining.

For detecting the signal of αB-crysyallin in cytoskeletal preparation, silver stain kit (Bio-Rad) was used to increase the protein sensitivity. After analysis of cytoskeletal preparation by SDS-PAGE, protein gel was incubated in 40% methanol and 10% acetic acid (v/v) at least 30 minutes. Then the fixed buffer was discarded and gel was incubated in sensitized buffer for 5 minutes. Last buffer was discarded and gel was washed in large volumes of milli-Q water for 2 minutes 3 times. Gel was then stained with staining buffer for 20 minutes. Again, staining buffer was discarded and gel was rinsed in milli-Q water for quickly 30 seconds. Finally, gel was developed in developer until the appearance of brown bands. Notice that, the developing time does not over than 15 minutes.

Chapter 3：Results

3.1 The effect of G154S αB-crystallin on the interaction with desmin filaments in vitro.

3.1.1 Expression and purification of recombinant G154S αB-crystallin.

The G154S αB-crystallin generated by site directed mutagenesis was used to produce recombinant protein suitable for subsequent in vitro studies. The G154S αB-crystallin was expressed in *Escherichia coli* BL21(DE3) pLysS strain using a pET-based vector system and purified to homogeneity by a two-step purification protocol [97]. The expression and purification of the G154S αB-crystallin was monitored by SDS-PAGE followed by staining with Coomassie Blue R250 (Fig. 1.1). In the first step, the G154S αB-crystallin was purified by anion exchange chromatography using a TMAE column. This step removed most of the contaminated proteins from bacteria. Results of a representative chromatographic profile are shown (Fig. 1.2). Complete removal of the impurities was achieved by subsequent gel filtration chromatography on a Sephacryl® S-400 HR column. A representative chromatogram and the elution profile of the column chromatography are shown (Fig. 1.3). Column fractions containing purified αB-crystallin were collected and protein concentrations were determined by bicinchonic acid (BCA) assay with use of bovine serum albumin as a standard (Fig. 1.4). The recombinant human desmin as well as wild type and R120G αB-crystallin were purified as described previously [53].

3.1.2 Interaction of αB-crystallin and desmin filaments in vitro.

Previous studies on DRM showed that the myopathic mutation R120G αB-crystallin caused cytoplasmic aggregates containing desmin IFs and αB-crystallin in muscle cells of affected individuals [56]. Structural studies have confirmed that the R120G mutation in αB-crystallin results in altered secondary, tertiary, and quaternary structure,

decreased protein stability and compromised chaperone function [54, 65, 98, 99, 100]. Using several in vitro assays, the effects of R120G mutant upon the interaction with astrocyte-specific IF protein glial fibrillary acidic protein [54] and desmin[53] had been studied previously. These results suggested that the major histopathological feature of the disease, namely, IF aggregates, could result from an altered interaction between αB-crystallin and IF proteins.

Cosedimentation has been very effective in showing the interaction of αB-crystallin with the assembled intermediate filaments [51]. Therefore this assay was used to investigate whether the G154S mutation in αB-crystallin alters its interaction with desmin filaments in vitro. A schematic view showing the basic principle of this assay is shown (Fig. 1.5). The binding of either wild type or G154S αB-crystallin with desmin filaments were determined by measuring the ratio of bound and unbound αB-crystallin to desmin at 37℃. Cosedimentation assay was performed at the molar concentrations range from 1:2 to 2:1 ratio of αB-crystallin to desmin. Protein amounts in the supernatant and pellet fractions were determined by densitometry. Representative cosedimentation data are shown in Figures 1-6 and 1-7. Under the conditions of the assay, desmin assembled efficiently and ~95% protein was found in the pellet fraction (Fig. 1.6A, lane 2, labeled P) with very little (~ 5%) detectable desmin left in the supernatant fractions (Fig. 1.6A, lane 1, labeled S). In the absence of desmin, both wild type (Fig. 1.6B, lanes 1, 3 and 5) and G154S (Fig. 1.7A, lane 9) αB-crystallin remained mostly soluble, with only ~10% of wild type (Fig. 1.6B, lanes 2, 4 and 6) and G154S (Fig. 1.7A, lane 10) αB-crystallin and being sediment into the pellet fractions. When desmin was included in the assay at 2:1, 1:1 and 1:2 molar ratios, 27% (Fig. 1.6B, lane 8), 31% (Fig. 1.6B, lane 10) and 43% (Fig. 1.6B, lane 12), respectively, of wild type αB-crystallin (Fig. 1.6B, lanes 10 and 12) compared with 28% (Fig. 1.7A, lane 4), 38% (Fig. 1.7A, lane 6) and 50% (Fig. 1.7A, lane 8), respectively, of G154S

αB-crystallin cosedimented with desmin filaments. These data suggest that the G154S αB-crystallin binds desmin filaments more efficiently than wild type protein in vitro.

3.1.3 Visualization of the interaction between αB-crystallin and desmin by electron microscopy.

To visualize the direct association of wild type or G154S αB-crystallin with the desmin filaments during the cosedimentation assays, samples were stained with 1% (w/v) uranyl acetate and examined by transmission electron microscope (Fig. 1.8). In the absence of desmin filaments, both wild type (Fig. 1.8C) and G154S (Fig. 1.8D) αB-crystallin formed discrete particles approximately 15–20 nm in diameter. When included in the coassembly assay, some of wild type αB-crystallin binding to desmin filament was observed (Fig. 1.8A). Similar results were obtained when the G154S αB-crystallinn coassembled with desmin filaments (Fig. 1.8B). These observations correlated well with the cosedimentation assay results (Fig. 1.6B and 1.7B), where both wild type and the G154S αB-crystallin partially bind to desmin filaments and the G154S αB-crystallin appears to bind more efficiently to desmin filaments.

3.2 The effect of αB-crystallin mutation on the IF networks in cultured cells determining.

To test whether the G154S mutation alters the interaction of αB-crystallin with desmin filament networks in cultured cells, BHK21 and C2C12 cells were transfected with G154S αB-crystallin and compared with those transfected with wild type protein. These cells were muscle-derived cell lines with desmin being expressed as a major IF protein and contain little endogenous αB-crystallin. Therefore, these cell lines provides an excellent experimental system to test the effect of the αB-crystallin mutation on the organization of the endogenous desmin IF networks.

To determine the distribution of αB-crystallin in relation to the endogenous desmin filament networks, BHK21 cells transfected with either wild-type, G154S or R120G

αB-crystallin were fixed at 48 hour posttransfection and processed for double label immunofluorescence microscopy. Cells transfected with wild-type αB-crystallin showed a cytoplasmic distribution (Fig. 2.1B) that is partially coaligned with bundles of desmin filaments (Fig. 2.1A). Similar observation on αB-crystallin distribution was observed (Fig. 2.1H) in cells transiently transfected with G154S αB-crystallin (Fig. 2.1I). In contrast, the majority of cells transfected with R120G αB-crystallin form perinuclear aggregates (Fig. 2.1E). These aggregates were not obviously desmin positive (Fig. 2.1D), although desmin filaments were usually around the periphery of these aggregates (Fig. 2.1F). These data show that cells expressing wild-type and G154S αB-crystallin exhibit cytoplasmic distribution of αB-crystallin. Expression of R120G mutant, however, leads to aggregate formation and the localized reorganization of desmin filaments, which are in agreement with previously published data where desmin filaments seemed to engulf the R120G-containing aggregates in transfected BHK21 cells [2, 3].

3.2.1 Expression level and solubility property of αB-crystallin.

The relative expression levels and solubility property of the wild-type and mutant αB-crystallin in transfected BHK21cells were determined by immunoblotting analysis. BHK21 cells express very low levels of the endogenous αB-crystallin as shown by the immunoblot analysis of untransfected cells using the anti-αB-crystallin antibody (Fig. 2.2A, lane 1). In contrast, cells transfected with either wild type (Fig. 2.2A, lane 2), R120G (Fig. 2.2A, lane 3) or G154S (Fig. 2.2A, lane 4) αB-crystallin generated proteins of the expected size at comparable levels. The solubility of the wild-type and mutant αB-crystallin were monitored by immunoblotting of the supernatant and pellet fractions prepared using a harsh extraction buffer containing deoxyclolate [94]. Under these extraction conditions, the endogenous αB-crystallin (Fig. 2.2B, lane 1) and transfected wild-type (Fig. 2.2B, lane 3) αB-crystallin were found entirely in the

soluble fraction of untransfected and wild-type αB-crystallin-transfected cells. Whilst the G154S αB-crystallin was also detected in the soluble fraction of G154S αB-crystallin (Fig. 2.2B, lane 7) tansfected cells, a significant proportion (~50%) of the R120G αB-crystallin was found in the pellet fraction (Fig. 2.2B, lane 5) in cells transfected with R120G αB-crystallin. Under the same extraction conditions, the endogenous desmin was found exclusively in the pellet fraction in untransfected (Fig. 2.2B, lane 2) and αB-crystallin-transfected cells (Fig. 2.2B, lanes 4, 6 and 8). These data suggest a limited association of G154S αB-crystallin with desmin intermediate filaments in transfected BHK21 cells. The R120G αB-crystallin apparently associated with desmin filaments and this association could contribute directly to the localized reorganization of the desmin filament network seen in the R120G αB-crystallin transfected BHK21 cells.

3.2.2 Expression of αB-crystallin in C2C12 cells.

The next important question to address is whether the distribution of αB-crystallin is independent of the cellular background. Transient transfection assays coupled with immunofluorescence microscopy were conducted to compare the distribution of wild-type and mutant αB-crystallin in the mouse myoblast C2C12 cells. This cell type expresses the endogenous desmin and low level of αB-crystallin and therefore would be expected to better mimic the disease scenario of mutant αB-crystallin being expressed in the muscle cell background. C2C12 cells were tansiently transfected with either wild-type or mutant αB-crystallin. At 48 hour after transfection, the distribution of αB-crystallin was examined by confocal immunofluorescence microscopy with use of a monoclonal antibody to αB-crystallin. When expressed in C2C12 cells, wild-type αB-crystallin showed cytoplasmic distribution (Fig. 2.3A), whereas, R120G αB-crystallin formed cytoplasmic aggregates (Fig. 2.3B). The G154S αB-crystallin appeared to show more filamentous staining pattern with beaded morphology (Fig.

2.3C). The distribution of wild-type or mutant αB-crystallin in relation to the endogenous desmin filament networks was examined by double label immunofluorescence microscopy (Fig. 2.4). Cells transfected with either wild-type or G154S αB-crystallin showed a cytoplasmic distribution (Fig. 2.4, A and I) that is partially coaligned with bundles of desmin filaments (Fig. 2.4, D and L). In contrast, the R120G αB-crystallin often form perinuclear aggregates in transfected cells (Fig. 2.4B), which were not obviously desmin positive (Fig. 2.4H).

The relative expression levels and solubility of wild-type and mutant αB-crystallin were determined by immunoblotting of extracts from C2C12 cells prepared using RIPA extraction buffer. Analysis of total lysates revealed little endogenous αB-crystallin expressed in nontransfected C2C12 cells (Fig. 2.5B, lane 1), whereas cells transfected with either wild type (Fig. 2.5B, lane 2) or mutant (Fig. 2.5B, lane 3-4) αB-crystallin generated proteins of the expected size. Under these extraction conditions, the endogenous (Fig. 2.5A, lane 1-2), wild type (Fig. 2.5A, lane 3-4) and G154S (Fig. 2.5A, lane 7-8) αB-crystallin were almost completely extracted from the untransfected, wild-type, and G154S αB-crystallin transfected cells, conditions that also extracted desmin. In contrast, a significant proportion (~50%) of R120G αB-crystallin remained in the pellet fraction in cells transfected with R120G αB-crystallin. When the supernatant and pellet fractions were also probed with antibody to phosphorylated αB-crystallin at Ser-59, a significant increase in the phosphorylated form of αB-crystallin was observed in the pellet fraction of R120G αB-crystallin transfected cells. The increased phosphorylation of αB-crystallin in R120G αB-crystallin transfected cells is not restricted to C2C12 cells, as similar results were observed when R120G αB-crystallin was transiently expressed in human breast carcinoma MCF7 cells that are epithelial in origin. This cell type expresses only keratin IF proteins but little endogenous αB-crystallin [53]. When expressed in this cell

line, both wild-type and mutant αB-crystallin generated proteins of the expected size at comparable levels (Fig. 2.6B, lanes 2-4). In contrast to untransfected (Fig. 2.6B, lane 1) or WT αB-crystallin-transfected (Fig. 2.6B, lane 2) cells, phosphorylated αB-crystallin levels were significantly increased in cells transfected with R120G αB-crystallin (Fig. 2.6B, lane 3). The level of phospho-αB-crystallin in G154S mutant-transfected cells (Fig. 2.6B, lane 4) was somewhat between these two extremes of the wild-type and R120G αB-crystallin. Analysis of the supernatant and pellet fractions revealed that both wild-type (Fig. 2.6A, lane 3) and G154S (Fig. 2.6A, lane 7) αB-crystallin were almost completely extracted from wild-type and G154S αB-crystallin-transfected cells. Under the same extraction conditions, almost all of the HSP70, HSP27 and actin were also extracted (Fig. 2.6A, lanes 3 and 7). In contrast, a significant proportion of R120G αB-crystallin resisted such an extraction and a significant proportion of the R120G protein still remained in the pellet fraction (Fig. 2.6A, lane 6). In R120G αB-crystallin-transfected cells, the phosphorylated αB-crystallin was detected in both the supernatant (Fig. 2.6A, lane 5) and pellet fractions (Fig. 2.6A, lane 6). To investigate whether aggregation of R120G αB-crystallin could adversely affect cell viability through activation of caspase 3, I also measured levels of activated caspase 3. Whilst inactive full-length caspase 3 was found exclusively in the supernatant fraction in wild-type and mutant αB-crystallin transfected cells, no active caspase 3 was detected in both untransfected and αB-crystallin-transfected cells.

As sHSPs are highly soluble proteins [101], αB-crystallin would be expected to be present exclusively in the supernatant fraction. With use of an extraction buffer containing deoxyclolate, both wild-type and G154S αB-crystallin were almost completely extracted from αB-crystallin-transfected cells. Although some R120G αB-crystallin was recovered in the insoluble fraction, a significant proportion of the R120G mutant remained soluble. Under the same extraction conditions, the

endogenous desmin was completely extracted into the supernatant fraction. The presence of desmin and αB-crystallin in the supernatant fraction raised the possibility that both were associated in a soluble complex. To test this hypothesis, a series of co-immunoprecipitation experiments was performed. In a pilot experiment, C2C12 or BHK 21 cells were first extracted with a mild extraction buffer containing 1% (v/v) Triton X-100 to preserve the potential protein-protein interactions. Under these extraction conditions, however, desmin was found mainly in the pellet fraction (Fig. 2.8A and B, lane 2 and 7) and soluble desmin in the supernatant fraction is not sufficient to perform immunoprecipitation. To increase the soluble form of desmin, cells were extracted with the radio-immunoprecipitation assay (RIPA) buffer containing both ionic and nonionic detergent. After extraction, the supernatant fraction containing soluble desmin was increased and used for subsequent co-immunoprecipitation assay. During the course of study, I found that the process of freeze and thaw of the supernatant fraction accelerates self-aggregate of soluble proteins including desmin, which precipitated easily even without centrifugation. To avoid this non-specific precipitation, standard immunoprecipitation experiment was performed using the soluble fraction obtained immediately after cell extraction. Using an anti-αB-crystallin antibody, protein complexes were immunoprecipitated from the RIPA-soluble fraction. The immunoprecipitated complexes were then probed with a panel of antibodies to αB-crystallin and desmin (Fig. 2.9). As expected, αB-crystallin can be immunoprecipitated by the anti-αB-crystallin antibody (Fig. 2.9, lanes 5~8), but co-immunoprecipitation of desmin was not detected.

Mitochondrial abnormalities contribute to the pathogenic process of DRM. This is supported by previous studies [81], in which expression of R120G αB-crystallin disrupted mitochondrial membrane potential, activated opening of the mitochondrial permeability transition pore and release of cytochrome c from mitochondria. Apoptotic

pathways are subsequently activated, which eventually results in cardiomyocyte death, dilation, and heart failure [81]. To investigate whether expression of the G154S αB-crystallin affects mitochondrial distribution, C2C12 cells were transfected with either R120G or G154S αB-crystallin. Cells transfected with wild type αB-crystallin were used as a control. The distribution of mitochondria in relation to transfected αB-crystallin was visualized by staining with mitochondrial-selective dye MitoTracker (Fig. 2.7, B, F and J). When transfected into C2C12 cells, both wild-type (Fig. 2.7, A) and G154S (Fig. 2.7, I) αB-crystallin exhibited a cytoplasmic staining pattern. In contrast, cells transfected with R120G αB-crystallin contained cytoplasmic aggregates (Fig. 2.7, E). Expression of either wild-type or mutant αB-crystallin did not cause redistribution of mitochondria, which were localised throughout the cytoplasm (Fig. 2.7, B, F and J). In cells transfected with wild-type or mutant αB-crystallin, the nuclear morphology appeared normal, as revealed by DAPI staining (Fig. 2.7, C, G and K).

3.3 Generation of stable cell lines.

Although transient transfection provides a quick and convenient way to analyze expressed proteins in cells, the transfection efficiency and expression levels varied between experiments. Therefore, stable cell lines provide a better experimental system to achieve a more consistent study. Prior to establishing cell line, it is important to titrate the selection antibiotics to determine the optimal concentration for selection with the particular host cell line being tested. In this study, BHK21 and C2C12 cells were selected, because these cell lines normally express the endogenous desmin and low levels of αB-crystallin. Therefore these cell lines would be expected to better mimic the disease scenario of DRM with mutant αB-crystallin being expressed in the muscle cell background. Initially, BHK21 cells were seeded in 10-cm tissue culture dishes containing growth medium supplemented with varying amount of G418 (500

or 1000 g/ml) and hygromycin (25, 50, 100, 200, 400 or 800 g/ml). Cells were cultured for 1-12 days and the selective medium was replaced every two days to maximize the efficiency of the antibiotics. Cell viability was monitored by visual assessment of adherent and floating cells every day. I have found 400 μg/ml G418 and 200 μg/ml hygromycin to be optimal for killing most of the BHK21 cells (Fig. 3.1) and these concentrations of antibiotics were used to select for antibiotic-resistant clones that express αB-crystallin.

To generate stable cell lines, BHK21 cells grown in 10 cm dishes at ~50% confluency were cotransfected with pcDNA3 vector containing either wither wild type or mutant αB-crystallin and the pTRE2-hyg vector. Two days after transfection, cells were dual selected with 400 μg/ml G418 and 200 μg/ml hygromycin for two weeks. After selection, antibiotic-resistant clones were isolated using cloning cylinders and transferred to 35 mm Petri dishes. Once the cells reached ~90% confluency, they were trypsinized and transferred to a 10 cm Petri dish to expand the culture.

3.3.1 Screening of BHK21 cell lines expressing αB-crystallin.

The expression levels of αB-crystallin in BHK21 stable clones were analyzed by immunoblotting. As a control, transient transfection was performed to analyze the expression levels of αB-crystallin. BHK21 cells transfected with either wild-type or R120G αB-crystallin were extracted with RIPA buffer. Analysis of the total cell lysates revealed that levels of αB-crystallin increased in αB-crystallin-transfected cells (Fig. 3.2B, lanes 2 and 3) compared to untransfected controls (Fig. 3.2B, lane 1). Several wild-type and R120G αB-crystallin clones were selected for screening αB-crystallin expression. Stable cell lines that express high levels of αB-crystallin compared to the endogenous baseline levels of parental cells were selected for further characterization (Fig. 3.2 and Fig. 3.3). Among these lines, the 2E5 and 2G4' clonal

lines were selected because they express approximately equal levels of wild-type and R120G αB-crystallin (Fig. 3.3). The name of stable clone was according to the rule that "'" means R120G αB-crystallin stable clone and the reverse means wild-type αB-crystallin. The distribution of wild type and R120G αB-crystallin in relation to the endogenous desmin networks was visualized by double-label immunofluorescence microscopy using anti-αB-crystallin and anti-desmin antibodies. Because there is currently no antibody available to distinguish the expressed human αB-crystallin from the endogenous mouse αB-crystallin in BHK21 cells, it was first necessary to titrate the antibody concentration to the point where the endogenous αB-crystallin appeared as background staining on the parental cells. When αB-crystallin levels are elevated in stable clones, the signal becomes obvious above background. Stable cell lines expressing wild-type or R120G αB-crystallin showed cytoplasmic distribution of αB-crystallin (Fig. 3.2 A, 3.3A, 3.5A, and 3.6A).

To determine the solubility property of αB-crystallin in stable cell lines, a two-step fractionation protocol using Triton X-100 buffer and high salt extraction buffer was performed. The resulting supernatant and pellet fractions prepared from 2E5 and 2G4' cell lines were separated by SDS-PAGE followed by Coomassie blue (Fig. 3.4A) and silver staining (Fig. 3.4C), from these data, it can be seen that vimentin is the major IF protein in the final pellet of high-salt buffer extraction although desmin was also detected at lower levels (Fig. 3.4A and 3.4C). Immunoblotting analysis revealed that most of the wild-type and R120G αB-crystallin were recovered in the Triton X-soluble fraction, whereas little desmin was detected in this fraction (Fig. 3.4B, labeled S1). The Triton-insoluble fraction was further extracted with high salt buffer containing 1.5M KCl and the resulting supernatant and pellet fractions were probed with antibodies to desmin and αB-crystallin. Whilst desmin was found in both the supernatant and pellet fractions after being extracted with high salt buffer (Fig. 3.4B,

labeled S2 and P), little wild-type and R120G αB-crystallin were detected in the Triton-insoluble fractions. These data suggest that in stable cell lines the R120G αB-crystallin shifts its equilibrium from insoluble toward soluble pools (Fig. 3.4D). This result is in stark contrast to previous studies, where the increased insolubility of R120G αB-crystallin in vitro and in cultured cells was the dramatic effect of this mutation.

3.3.2 Screening of C2C12 cell lines expressing αB-crystallin.

After selection of C2C12 stable clones, the expression level of wild-type, R120G, and G154S αB-crystallin (Fig. 3.7 lane 1-4) was analyzed by immunoblotting. Also, the distribution of αB-crystallin was stained with monoclonal anti-αB-crystallin antibodies (Fig. 3.7 A-C). These data confirm again that wild-type αB-crystallin shows a normally cytoplasmic distribution throughout the cell (Fig. 3.7A), whereas, R120G αB-crystallin formed cytoplasmic aggregates (Fig. 3.7 B). The G154S αB-crystallin appeared to show beaded morphology.

Chapter 4：Disscussion

4.1 Interaction between desmin and αB-crystallin.

I have already shown that the increased interaction of desmin and R120G αB-crystallin by in vitro assay and indirect immunofluorecience. There have also many reports suggesting that the direct binding of desmin and R120G αB-crystallin. Co-immunoprecipitation was another method to support these data, although I tried hard to find out the suitable condition but didn't work out so far. R120G αB-crystallin not only decreased self-solubility but also compromised desmin filament network which leads to aggregate formation in cell model. Even cell lysate was extracted with high stringent buffer, R120G αB-crystallin was found lots amount in insoluble fraction. The key factor was that retained desmin in soluble fraction and also contained adequate amounts. Using high stringent buffer to extract cell lysate facilitates that increases solubility of desmin. But at the same time, the protein-protein interaction may break by detergent. However, extraction of cell lysate by using low stringent buffer could maintain the protein-protein interaction but not used upon increased desmin solubility. Indeed, Co-IP was limited that using soluble fraction to investigate the interaction of desmin and αB-crystallin due to prevent the nonspecific interaction. Although I have yet try that using total lysate to process Co-IP experiment, but cell lysate may treated with 5,000rpm, which lower than 12,000rpm and higher than no treated (Total lysate), then extracted with low stringent buffer. Until now, there has no published data and well established protocol interpret that the differential binding affinity to desmin between wild type and mutant αB-crystallin. Because the main reason was αB-crystallin was a highly soluble protein but not desmin. In signaling pathway, I observed R120G αB-crystallin was apparently phosphorylated on Ser^{59} site in the pellet fraction in C2C12 cells but both in supernatant and pellet in

MCF7 cells. This data indicated that the phosphorylated form of αB-crystallin may decrease its solubility. Both in C2C12 and MCF7 cells, R120G αB-crystallin was highly phosphorylated on Ser^{59} site, which is reported that this post-translational modification could modify the structure and functional property of αB-crystallin. That is the anti-apoptosis function was deficiency and may lead to apoptosis, although we have yet observed this phenomenon. So I could follow this clue and trace this potential signal pathway.

4.2 Establishment of stable cell line.

The expression levels of αB-crystallin in stable clone were shown in figure 3. BHK21 cell line only contained little endogenous αB-crystallin, so it provided distinguishability between endogenous αB-crystallin and transfected αB-crystallin. Unexpectably, the expression level of selected cells was too low compared to transiently transfectional cells. I also constructed in C2C12 stable clone recently, but similar results were appeared that C2C12 stable clones do not express αB-crystallin more than transiently transfection (Figure 3-7). The reason stable clone selection not efficient has been explained in result 3.3. To conduct high quality stable clone, there has another way to pick up the cells. I tried to select cells expressing αB-crystallin by insertion of dsRed sequence to the expression vector, which could excite red fluorescence when expressing in cells. And the flow cytometry was used to select cells which have red fluorescence exciting by laser beam. There has no efficient selection so far, but I think this progress was worth to continue.

4.3 The event which transfected αB-crystallin into cell model related to late onset disease of DRM.

DRMs are usually adult-onset neuromuscular diseases characterized by large accumulations of aggregates containing cytoplasmic desmin with other proteins [65]. There are many published data indicated that the R120G αB-crystallin could not only

alter the desmin filament status and simultaneously cause abnormal aggregate formation but also compromise mitochondrial distribution and consequent dysfunction and probably induce autophagy or apoptosis in mouse model and in patients [81, 89]. In my study, I observed the first response to cellular stress causing by R120G mutation in directly perturbing desmin filamentous structure. In cell model, cells were only transfected with mutant αB-crystallin for 48 hours. After fixed cells transfected with αB-crystallin, there has many cells contained R120G αB-crystallin-possitive aggregates, but also many cells contained normally desmin filament and expressed R120G αB-crystallin. This appearance indicated that I can't control the transfection efficiency. That's why I tried to establish wild type and mutant αB-crystallin stable cell line also an over expression of αB-crystallin system. However, I observed the change of mutant αB-crystallin base on their structure upon the ability of binding to desmin filament although I did not see other effect on autophagy and apoptosis in cell model.

Appendix

Appendix 1. IFs are classified into five major families.

IF proteins	Type	Molecular weight (kDa)	Assembly group	Distribution
Karatin (acidic)	I	40-64	A	Epithelia
Karatin (basic)	II	52-68	A	Epithelia
Vimentin	III	55	B	Heterogeneous
Desmin	III	53	B	Muscle
GFAP	III	50-52	B	Astrocyte/glia
Peripherin	III	54	B	PNS neurons
NF-L	IV	62	B	CNS neurons
NF-M	IV	102	B	CNS neurons
NF-H	IV	110	B	CNS neurons
α-internexin	IV	66	B	CNS neurons
lamin A/C	V	72/62	C	Nucleus
lamin β1	V	65	C	Nucleus
laminβ2	V	78	C	Nucleus

Appendix 2. Model of IF assembly

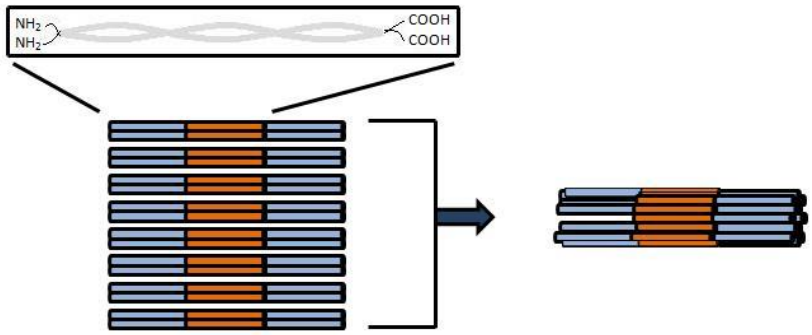

Phase1 : Tetramer forms into ULFs.

Phase 2 : Longitudinal annealing of ULFs into loosely packed filaments.

Phase 3 : Loosely packed filaments organized to yield 10nm IFs.

Appendix 3. Draw of desmin mutations

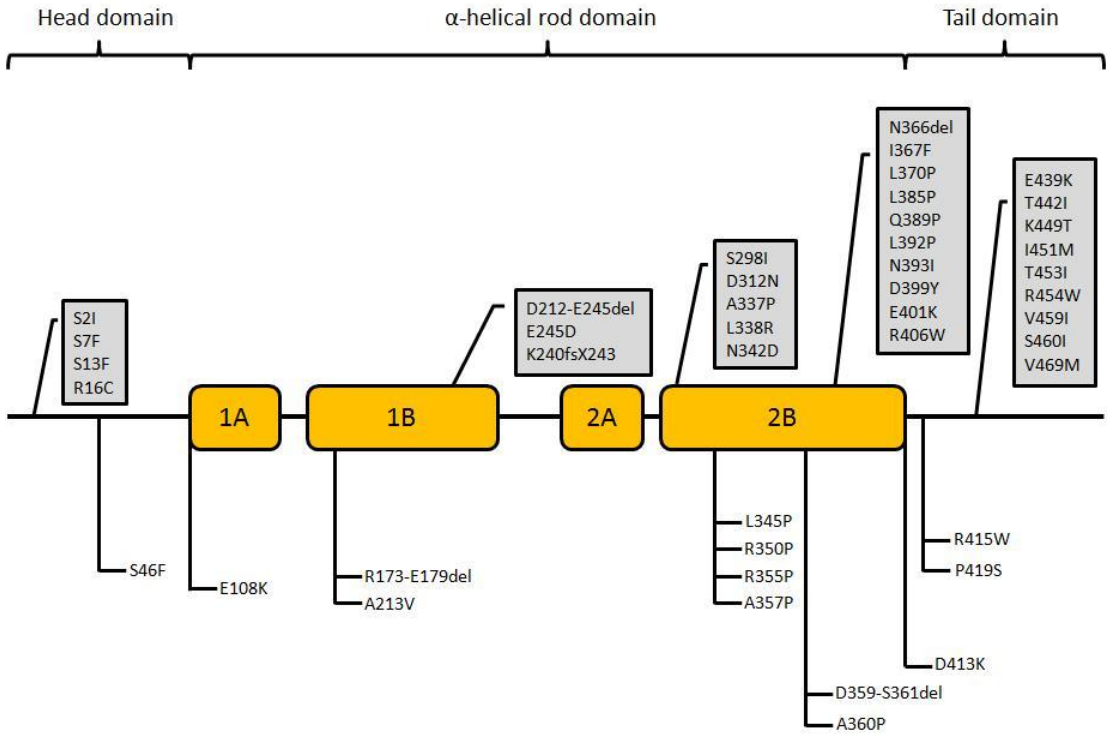

Figures

Figure 1-1. Electrophoretic analysis of expression and purification of G154S αB-crystallin.

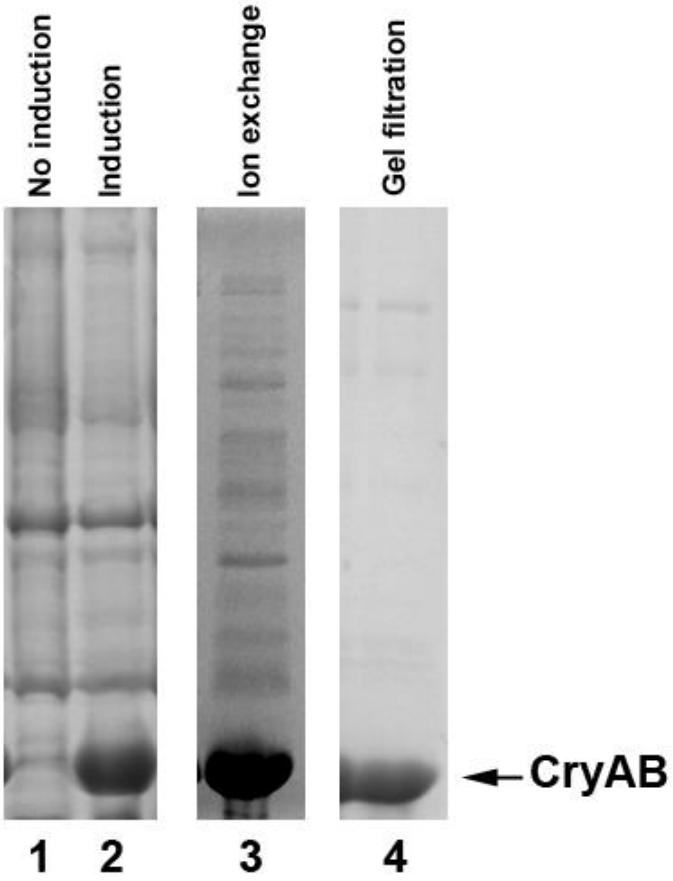

Figure 1-1. Electrophoretic analysis of expression and purification of G154S αB-crystallin. The G154S αB-crystallinin pET23d was transformed into *Escherichia coli* BL21pLysS strain. After transformation, protein expression was induced by the addition of 1 mM IPTG. Total protein profiles of uninduced (Lane 1) and induced (Lane 2) bacterial protein extracts are shown. The G154S αB-crystallin was purified to homogeneity by ion exchange (Lane 3) and gel filtration (Lane 4) chromatography.

Figure 1-2. Purification of G154S αB-crystallin by anion exchange chromatography.

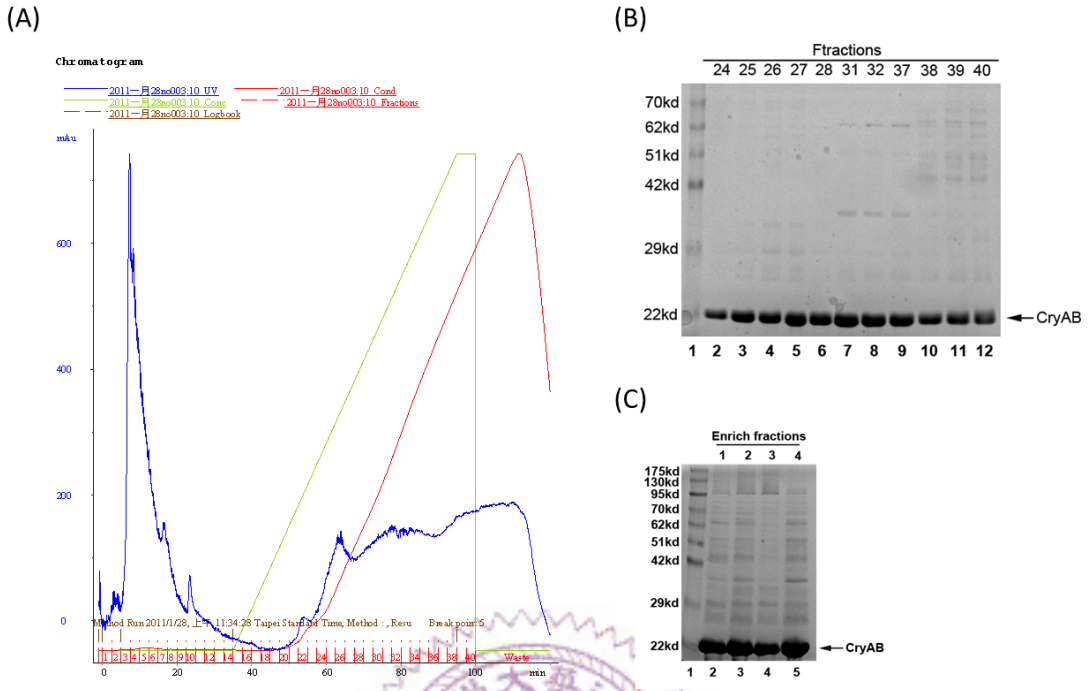

Figure 1-2. Purification of G154S αB-crystallin by anion exchange chromatography. The cleared supernatant prepared from bacterial extracts was applied into a DEAE Sepharose column pre-equilibrated in the column buffer A. After being washed with 6 bed-volume of the column buffer A, proteins were eluted from the column with a 0-1 M NaCl in the same buffer at a flow rate of 1 ml/min over 1 hour at room temperature. The chromatogram was showed (A). A small aliquot of protein sample from each fraction (B, lane 2~12) was analyzed by 12% (w/v) SDS-PAGE followed by Coomassie Brilliant Blue R250 staining (B). The G154S αB-crystallin-enriched fractions were pooled (C, lane 2~5), concentrated by centrifugal device (Millipore) and purified further by gel filtration chromatography.

Figure 1-3. Purification of G154S αB-crystallin by gel filtration chromatography.

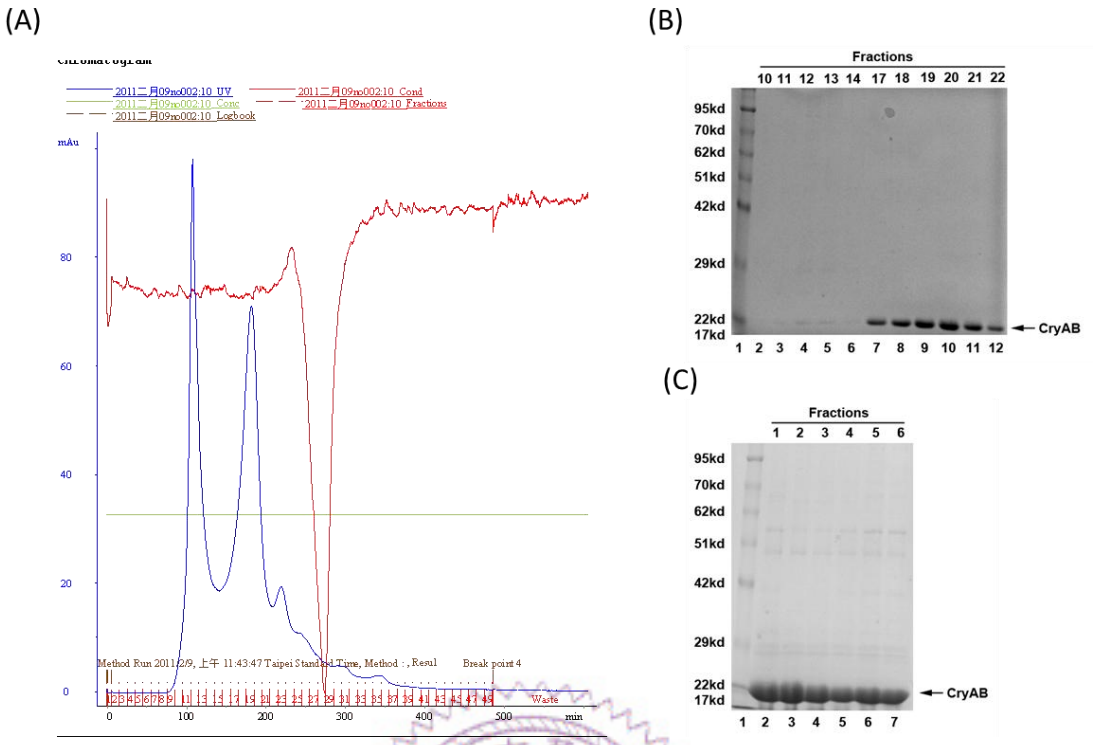

Figure 1-3. Purification of G154S αB-crystallin by gel filtration chromatography. An 1-ml concentrated protein sample was applied to a Sephacryl® S-400 HR column (1.6 x 60 cm) pre-equilibrated in column buffer B. The column was developed with the same buffer at a flow rate of 0.5 ml/min over 1 hour at room temperature and the elution profile was shown (A). Approximately 2 ml/tube was collected and the purity of αB-crystallin was analyzed by SDS-PAGE (B, 2~12). Each fractions were then enriched by passing centrifugal device (Millipore) as shown in (C, 2~7). A Coomassie Brilliant Blue-stained gel of protein samples from each fraction was shown. Molecular weight markers are shown in the lane 1 and the position of αB-crystallin is indicated by an arrow.

Figure 1-4. Protein concentration determination.

(A)

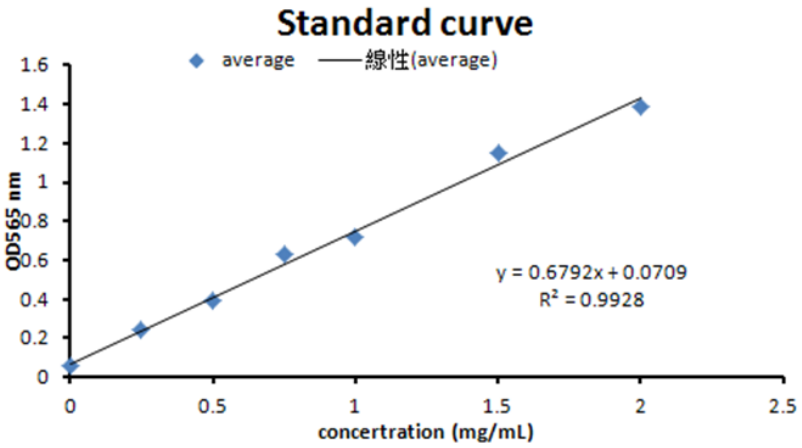

(B)

	OD565-1	OD565-2	(-)blank-1	(-)blank-2	AVE	Final concentration(mg/ml)
G154S-1	0.832	0.833	0.792	0.793	0.793	2.125
G154S-2	0.753	0.877	0.713	0.837	0.775	2.073
G154S-3	0.711	0.79	0.671	0.75	0.711	1.883
G154S-4	0.623	0.624	0.583	0.584	0.584	1.509
G154S-5	0.83	0.787	0.79	0.747	0.769	2.054
G154S-6	0.636	0.759	0.596	0.719	0.658	1.727

Figure 1-4. Protein concentration determination. After purification, the concentration of purified αB-crystallin was determined by bicinchoninic acid (BCA) assay. A standard curve was prepared by a series of dilution of known concentrations of standard protein, including 0.25, 0.5, 0.75, 1.0, 1.5 and 2 mg/ml of bovine serum albumin (BSA). A sample without any protein was used as a blank. A working reagent was first prepared by mixing 50 parts of Reagent A with 1 part of Reagent B. An aliquot of 200 ml working reagent was then added to microplate wells that contain 25 µl of each BSA standard and unknown sample replicates. After mixing thoroughly for 30 seconds, the plate was incubated at 37℃ for 30 minutes. The absorbance was measured at a wavelength of 565 nm on a microplate reader. The concentration of αB-crystallin in each fraction (B) was determined against the standard curve (A) generated by a series dilution of known concentrations of bovine serum albumin.

Cosedimentation assay explained

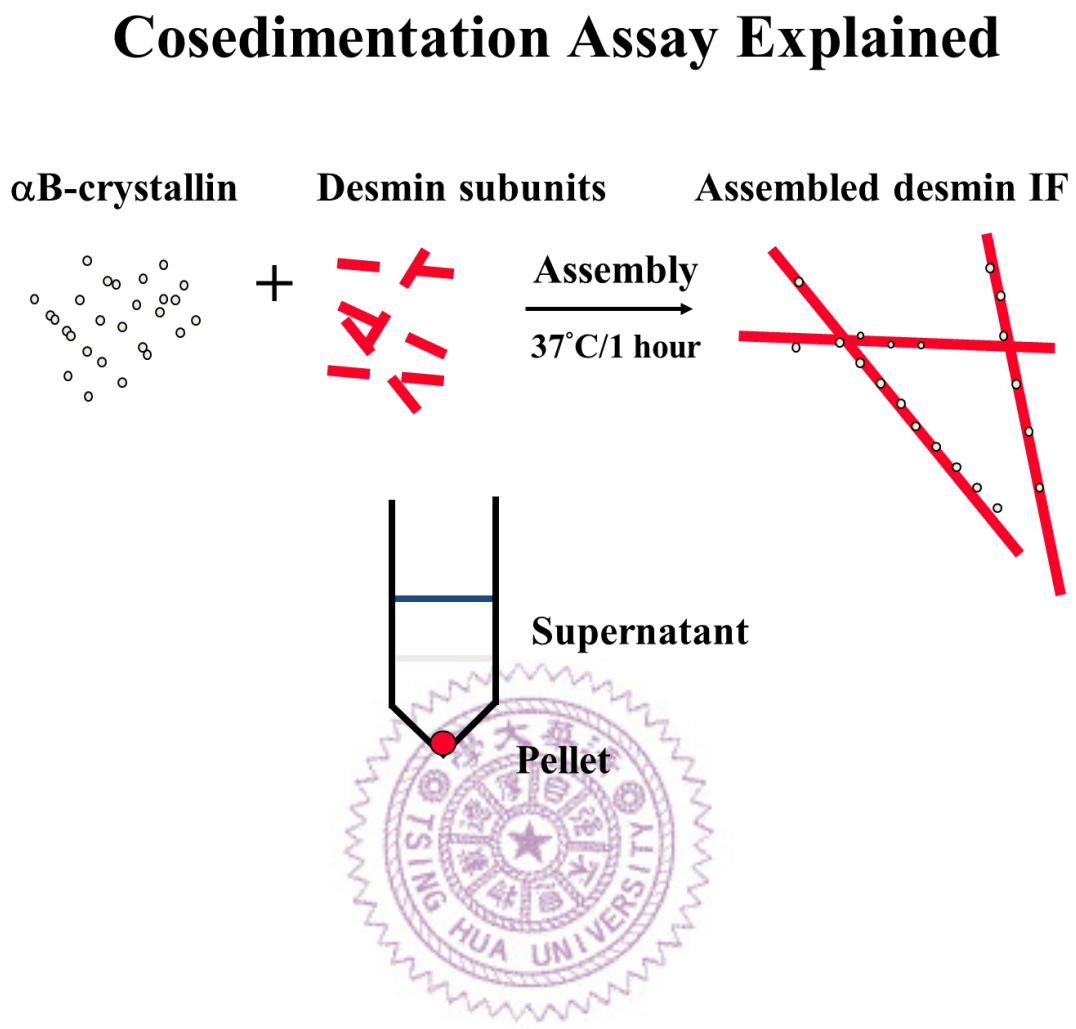

Figure 1-5.Cosedimentation of WT αB-crystallin with wild-type desmin in vitro.

(A) (B)

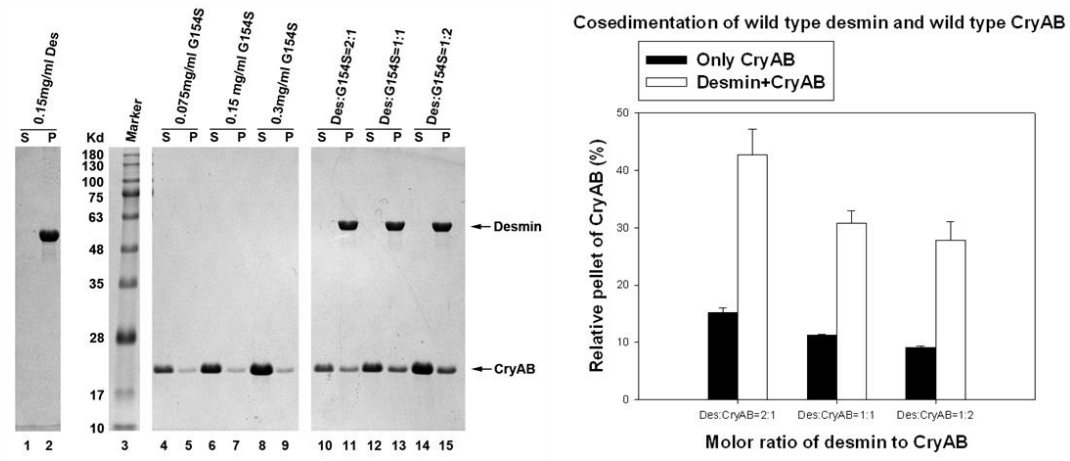

Figure 1-5.Cosedimentation of WT αB-crystallin with wild-type desmin in vitro. Desmin was assembled with additions of wild-type αB-crystallin (B) at indicated molar ratios at 37℃. The supernatant (S) and pellet (P) fractions were analyzed by SDS-PAGE followed by Coomassie Blue staining. Representative gels from the cosedimentation assay are shown (A). The positions of desmin, wild-type and G154S αB-crystallin are indicated. Under these assay conditions, desmin assembled efficiently as all proteins were found in the pellet fractions (A, lanes 11, 13, and 15, labeled P). In the absence of desmin, both the WT and G154S αB-crystallin remained mostly in the supernatant (A, lanes 4, 6, and 8, labeled S) with only ~10% being sedimented into the pellet fractions (A, lanes 5, 7, and 9, labeled P). When desmin was included in the assay, both the WT (A) and G154S αB-crystallin (Figure 1-6, A) cosedimented with desmin filaments in a concentration-dependent manner because increasing proportions of αB-crystallin were found in the pellet fractions at elevated ratios of αB-crystallin. The amounts of αB-crystallin and desmin in the supernatant and pellet fractions were quantified as described in MATERIALS AND METHODS. Quantification results from three independent experiments are shown as mean ± SE and presented as bar charts (B).

Figure 1-6. G154S αB-crystallin cosediment with wild-type desmin filament.

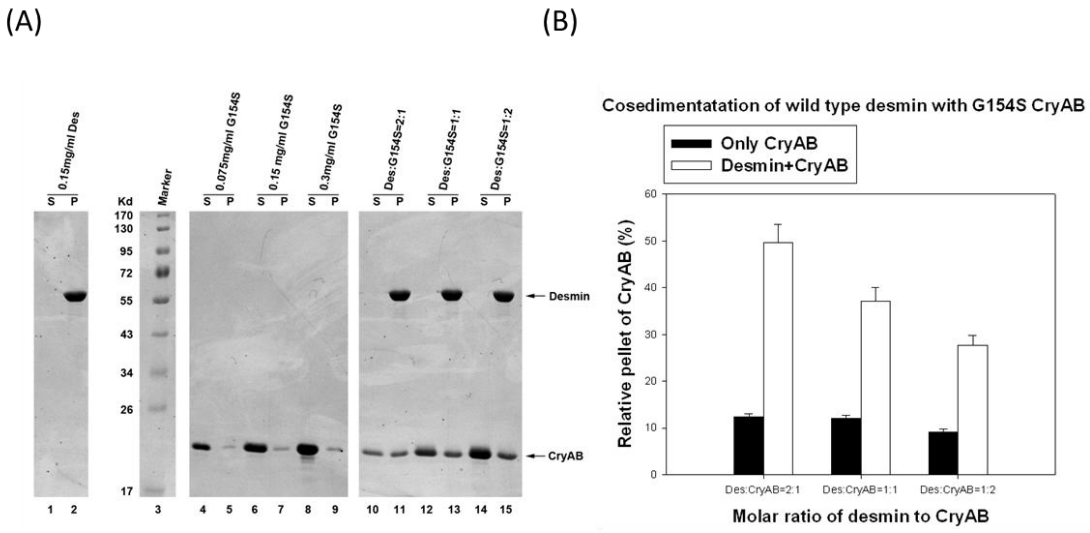

Figure 1-6. G154S αB-crystallin cosediment with wild-type desmin filament. After desmin was assemble ether individually or with additional G154S αB-crystallin at indicated molar ratios at 37℃ (B), protein samples were sediment at 32000 rpm for 30 minutes at 20℃. The resulting supernatant (S) and pellet (P) were analyzed by 12% SDS-PAGE followed coomassie blue staining as shown in (A). The molecular weight of desmin and αB-crystallin compared against commercial marker as shown in lane 3 and indicated by arrows. Assembly and consequent sedimentation of individual desmin and G154S αB-crystallin were displayed in lane 1~2 and lane 4~9. According to SDS-PAGE, desmin was assemble efficiently and almost found in P, reversely, over than 80 % of G154S αB-crystallin was found in S. Desmin and G154S αB-crystallin were assembly together and consequently cosediment at three different molar ratios were shown in (A, lane 10~15). In contrast to cosedimentation of desmin and wild-type αB-crystallin, G154S αB-crystallin has an increased more 10% of amounts than wild-type αB-crystallin were found in P. Quantified data from three independent experiments are shown as mean ± SE and presented as bar charts (B).

Figure 1-7. Visulization of WT and G154S αB-crystallin binding to desmin intermediate filaments in vitro by electron microscopy.

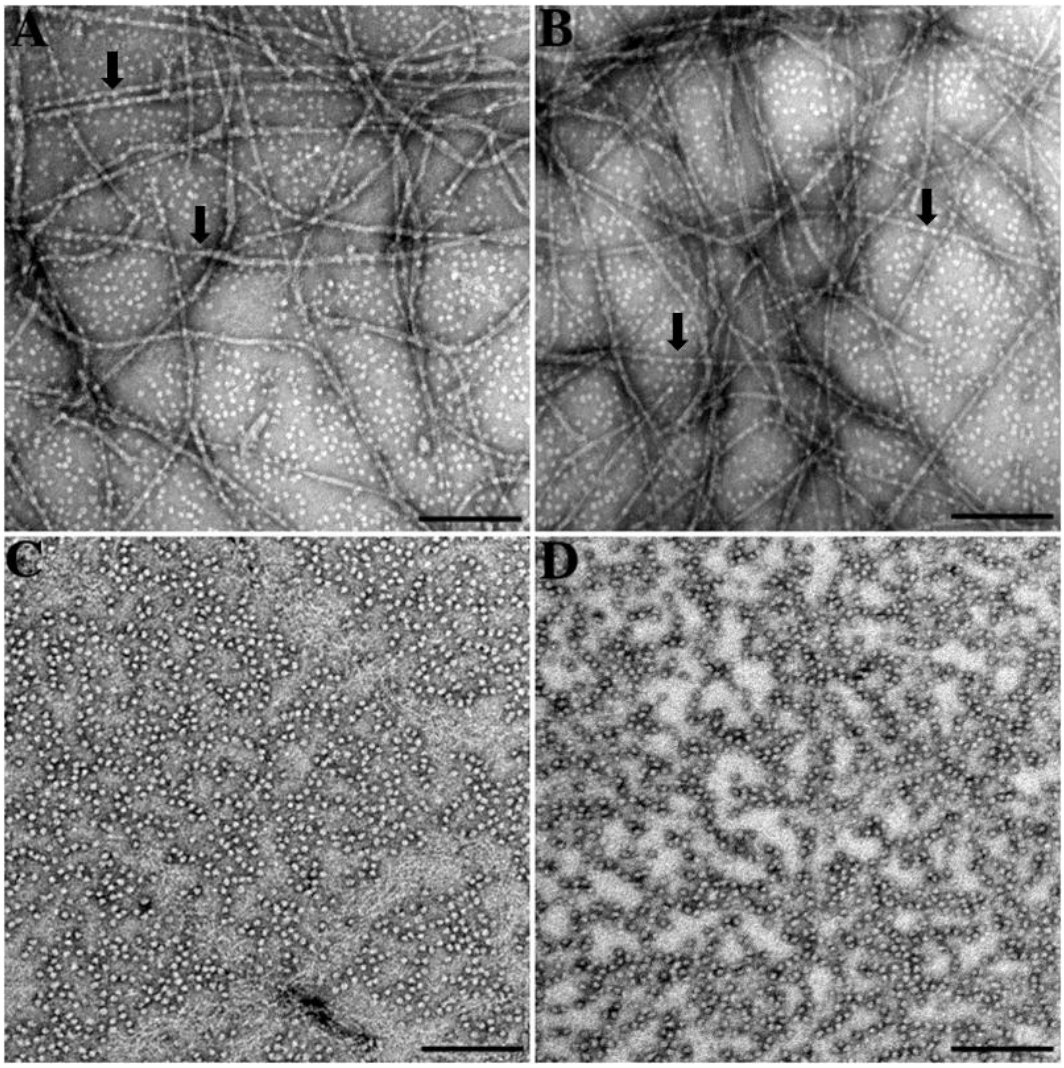

Figure 1-7.Visulization of WT and G154S αB-crystallin binding to desmin intermediate filaments in vitro by electron microscopy. Desmin was assembled in the presence of either WT (A), or G154S (B) αB-crystallin at 37℃ for 1 h. After assembly, protein samples were negatively stained with 1% (w/v) uranyl acetate and examined by electron microscopy. Under these assembly conditions, desmin formed typical 10-nm filaments with several microns in length (A). In the presence of WT αB-crystallin, desmin filaments had some αB-crystallin particles attached (B, arrows). Similar results were observed when G154S αB-crystallin was included in the coassembly mixture. In the absence of desmin, WT (C) and G154S (D) αB-crystallin both formed 15-20 nm particles. All micrographs are at the same magnification. Bar, 200 nm.

Figure 2-1. Formation of cytoplasmic aggregates in BHK21 cells expressing mutant αB-crystallin.

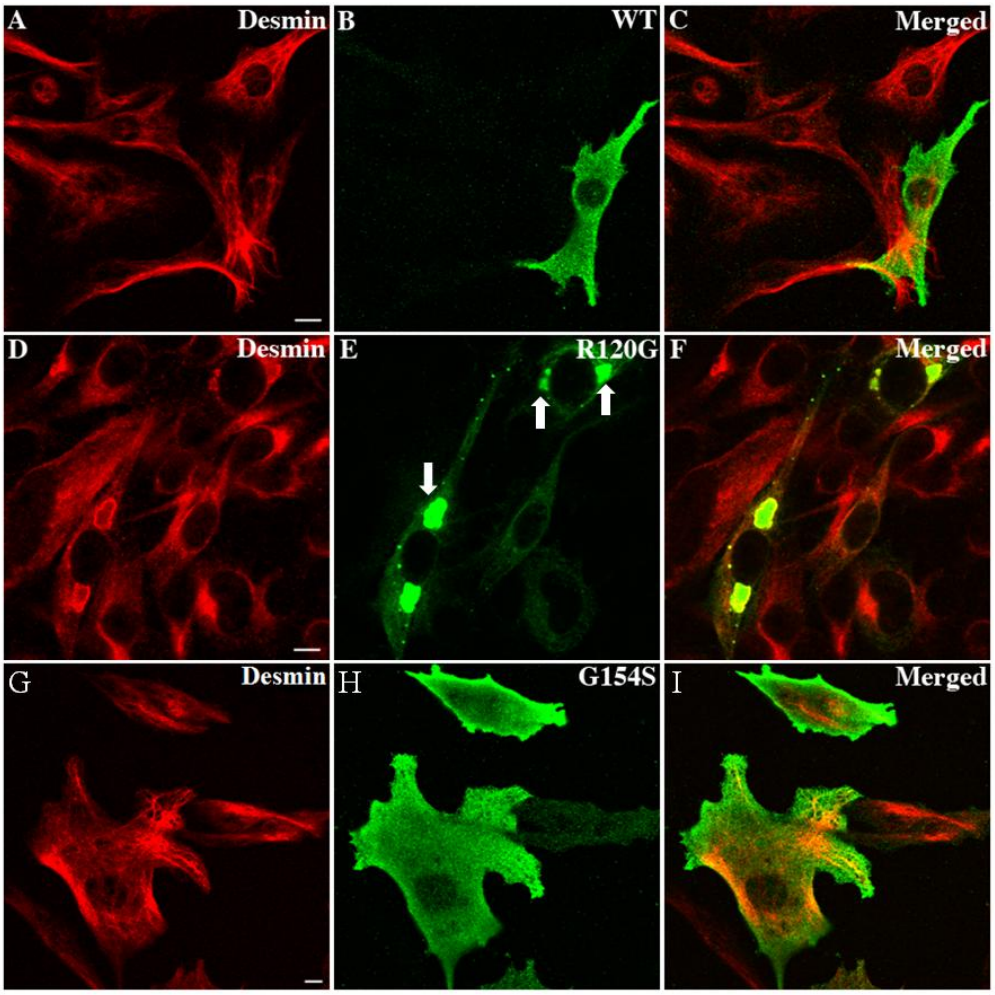

Figure 2-1. Formation of cytoplasmic aggregates in BHK21 cells expressing mutant αB-crystallin. BHK21 cells transiently transfected with either wild-type (A–C), R120G (D–F) or G154S (G-I) αB-crystallin were fixed at 48 hours after transfection. Subcellular distribution of αB-crystallin (B, E and H, green channel) in relation to desmin (A, D and G, red channel) was visualized by double labeling with use of monoclonal anti-αB-crystallin and polyclonal anti-desmin antibodies. Merged images show the superimposition of the green and red signals with areas of overlap in yellow (C, F and I). Images were acquired by a confocal laser scanning microscope. Cells expressing WT (B) and G154S (H) αB-crystallin showed cytoplasmic distribution of αB-crystallin and desmin. In contrast, cells expressing R120G αB-crystallin (E) resulted in the formation of cytoplasmic aggregates (white arrow) that are immunopositive for both αB-crystallin (E) and desmin (D). Notice that desmin-positive signals were distributed outside, but not within, the aggregates (F). Bar, 10 μm.

Figure 2-2. Analysis of wild type and mutant αB-crystallin in transiently transfected BHK21 cells by immunoblotting.

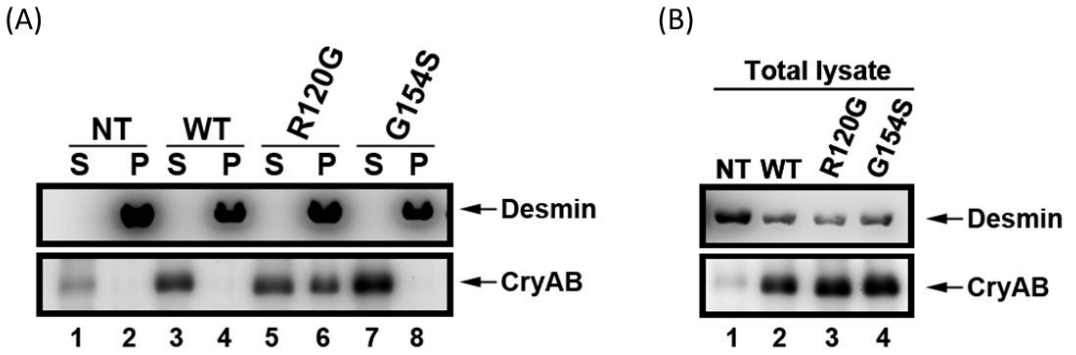

Figure 2-2. Analysis of wild type and mutant αB-crystallin in transiently transfected BHK21 cells by immunoblotting. BHK21 cells were transfected with either wild-type (B, lane2), R120G (B, lane 3) or G154S αB-crystallin (B, lane 4). Untransfected cells (B, lane 1) were used as a control. At 48 hours after transfection, cells were lysed on ice with triton X-100 extraction buffer. A small aliquot of total cell lysate was mixed with Laemmli sample buffer and the remaining lysate was subjected to centrifugation at 12,000 rpm at 4˚C for 10 minutes. The total cell lysates and resulting supernatant (S) and pellet (P) fractions were separated by SDS-PAGE and analyzed by immunoblotting using antibodies to desmin and αB-crystallin. The pellet fractions were dissolved in 125 μl Laemmli buffer which means enrich 8 times. The blot was developed by chemiluminescence system. Equal loading of various fractions were confirmed by probing with anti-actin antibody. Notice that whereas WT and G154S αB-crystallin were present almost entirely in the soluble fraction (B, lane 3 and 5, labeled S), ~50% of R120G αB-crystallin was found in the pellet fraction (B, lane 6, labeled P). Desmin immuno-positive signals were detected exclusively in the pellet fractions (A, lanes 2, 4, 6, and 8, labeled P).

Figure 2-3. Effect of C2C12 cells transiently transfected with either wild type αB-crystallin (A), or R120G αB-crystallin (B), or G154S αB-crystallin (C) after 48 hours.

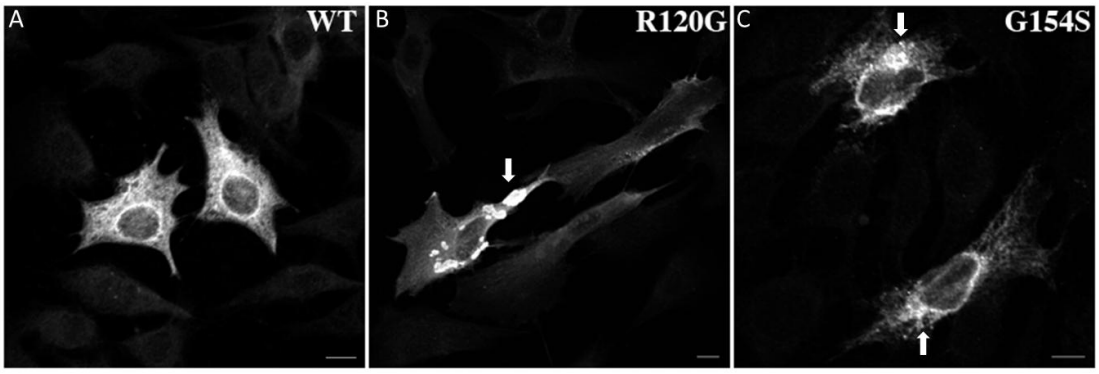

Figure 2-3. Effect of C2C12 cells transiently transfected with either wild type αB-crystallin (A), or R120G αB-crystallin (B), or G154S αB-crystallin (C) after 48 hours. G154S, which is published recently in 2010 in C2C12 cells and processed by immunofluorescence staining method. The αB-crystallin distribution werelabeled with monoclonal anti-αB-crystallin (A~C) which is the green channel. Images were showed that wild type αB-crystallin formed normally distribution throughout the cell (A), but unlikely, R120G αB-crystallin, which significantly formed intracellular aggregates, G154S αB-crystallin, which exhibited differently status from wild type and R120G αB-crystallin. G154S αB-crystallin tended to accumulate around the nuclear and existed in a small particle pattern, which .Bar, 20 μm.

Figure 2-4. Distribution of WT and mutant αB-crystallin in relation to the endogenous desmin IF networks.

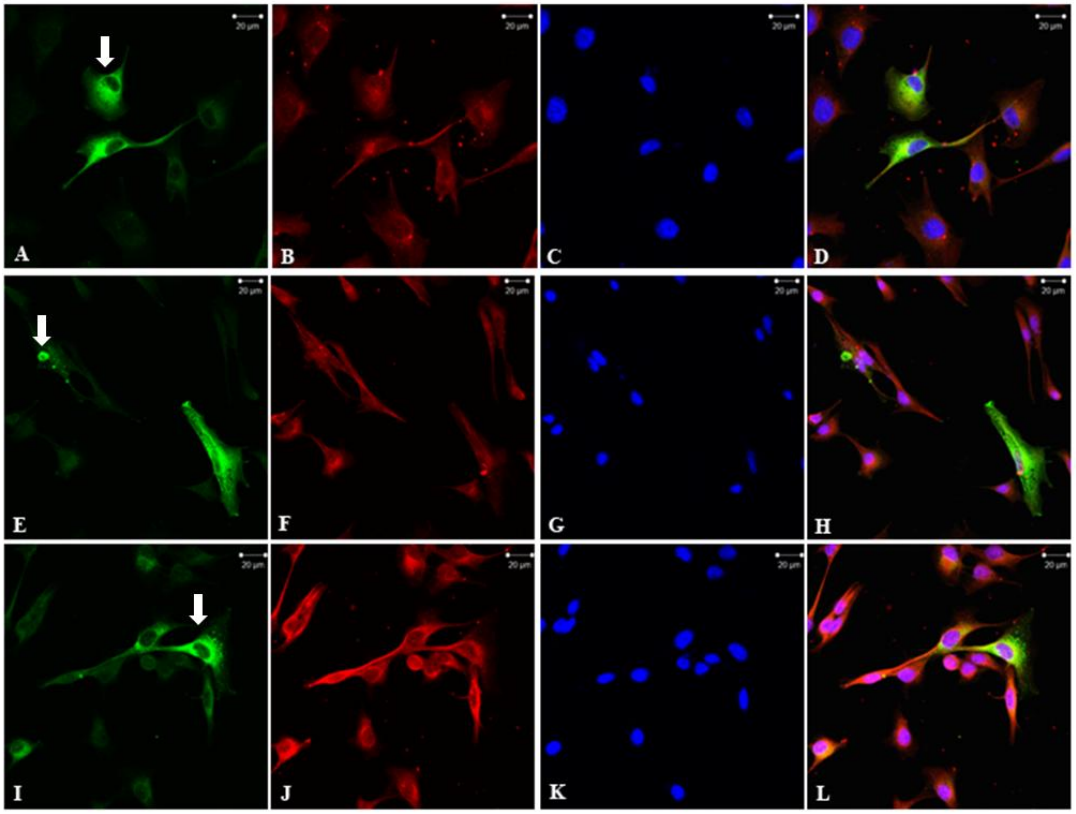

Figure 2-4. Distribution of WT and mutant αB-crystallin in relation to the endogenous desmin IF networks. C2C12 cells were transiently transfected with either wild type (A~D), R120G (E~H) or G154S (I~L) αB-crystallin. At 48 hours after transfection, cells were visualized by double labeling with anti-desmin (B, F, and J) and anti-αB-crystallin antibodies (A, E, and I). The immunofluorescence for αB-crystallin is in the green channel (A, E, and I), whereas the staining for desmin is in the red channel (B, F, and J). The nuclei were visualized by counterstaining with DAPI (C, G and K). Merged images show the superimposition of the green and red signals with areas of overlap in yellow. Images were acquired by a confocal laser scanning microscope. Cells expressing WT and G154S αB-crystallin showed cytoplasmic distribution of αB-crystallin (D) and desmin (L). In contrast, cells expressing R120G αB-crystallin resulted in the formation of cytoplasmic aggregates in some transfected cells (E, arrow). Bar, 20 μm.

Figure 2-5. Wild-type and mutant αB-crystallin were transiently transfected into C2C12 cells.

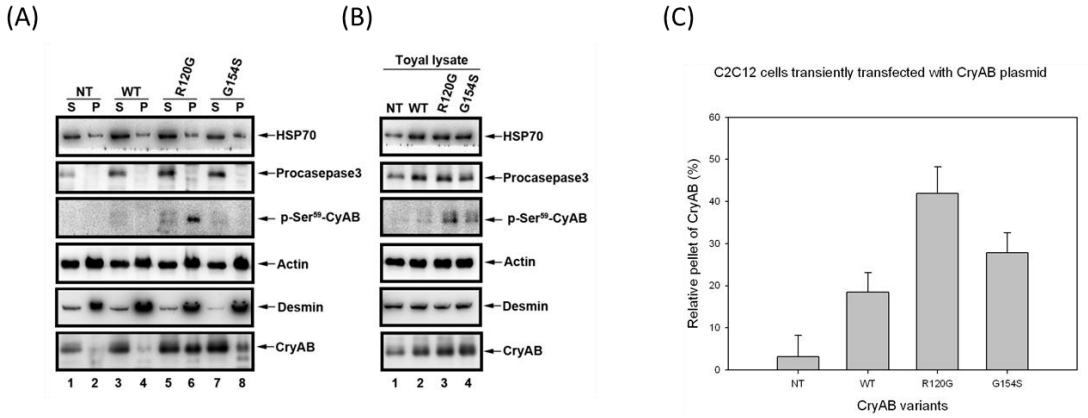

Figure 2-5. Wild-type and mutant αB-crystallin were transiently transfected into C2C12 cells. At 48 hour after transfection, the total cell lysates, supernatant (S) and pellet (P) fractions were prepared from these cultures and were compared with untransfected cells (B, lane 1). The pellet fractions were dissolved in 125 μl Laemmli buffer which means enrich 8 times. Immunoblots of the cell fractions were probed with antibodies to desmin, HSP70, αB-crystallin and phospho-αB-crystallin (p-Ser^{59}), procaspase 3, and finally actin, which was used as a loading control. When cells were transfected with R120G αB-crystallin, a significant proportion of the αB-crystallin but not HSP70 remained in the pellet fraction. Notice that the insoluble R120G αB-crystallin was phosphorylated on Ser-^{59} as detected by p-Ser^{59} phospho-specific antibody. The solubility of transfected wild type (A, lane 3 and 4), R120G (A, lane 5 and 6), and G154S αB-crystallin (A, lane 7 and 8) were compared with endogenous αB-crystallin (A, lane 1 and 2) in the C2C12 cell. The proportion of αB-crystallin amounts in pellet was quantified from three independent experiments are shown as mean ± SE and presented as bar charts (C).

Figure 2-6. Immunoblotting analysis of wild type and mutant αB-crystallin expressed in MCF7 cells.

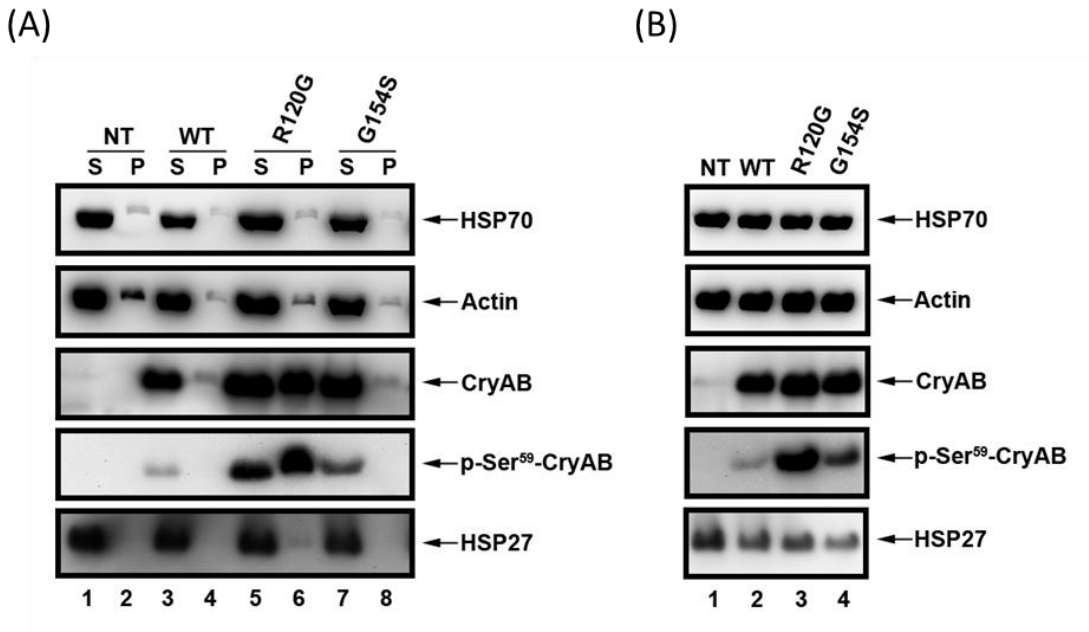

Figure 2-6. Immunoblotting analysis of wild type and mutant αB-crystallin expressed in MCF7 cells. MCF7 cells were either untransfected (A, lanes 1 and 2) or transfected with indicated αB-crystallin constructs. At 48 hours after transfection, cells were extracted on ice with RIPA buffer followed by centrifugation at 12,000 rpm at 4℃ for 10 minutes. The total cell lysates as well as the resulting supernatant (S) and pellet (P) fractions were separated by SDS-PAGE followed by immunoblotting with antibodies to HSP70, HSP27, αB-crystallin, phosphorelated form of αB-crystallin (p-Ser^{59}-αB-crystallin) and finally actin, which was used as a loading control. The pellet fractions were dissolved in 125 μl Laemmli buffer which means enrich 8 times. The blot was developed by enhanced chemiluminescence system. Notice that after transfection into MCF7 cells, both WT and mutant αB-crystallin expressed at comparable levels. Whereas WT (A, lane 3) and G154S αB-crystallin (A, lane 7) were present almost exclusively in the soluble fraction, ~50% R120G αB-crystallin was found in the pellet fraction.

Figure 2-7. Effect of αB-crystallin mutations upon mitochondrial distribution in C2C12 cells.

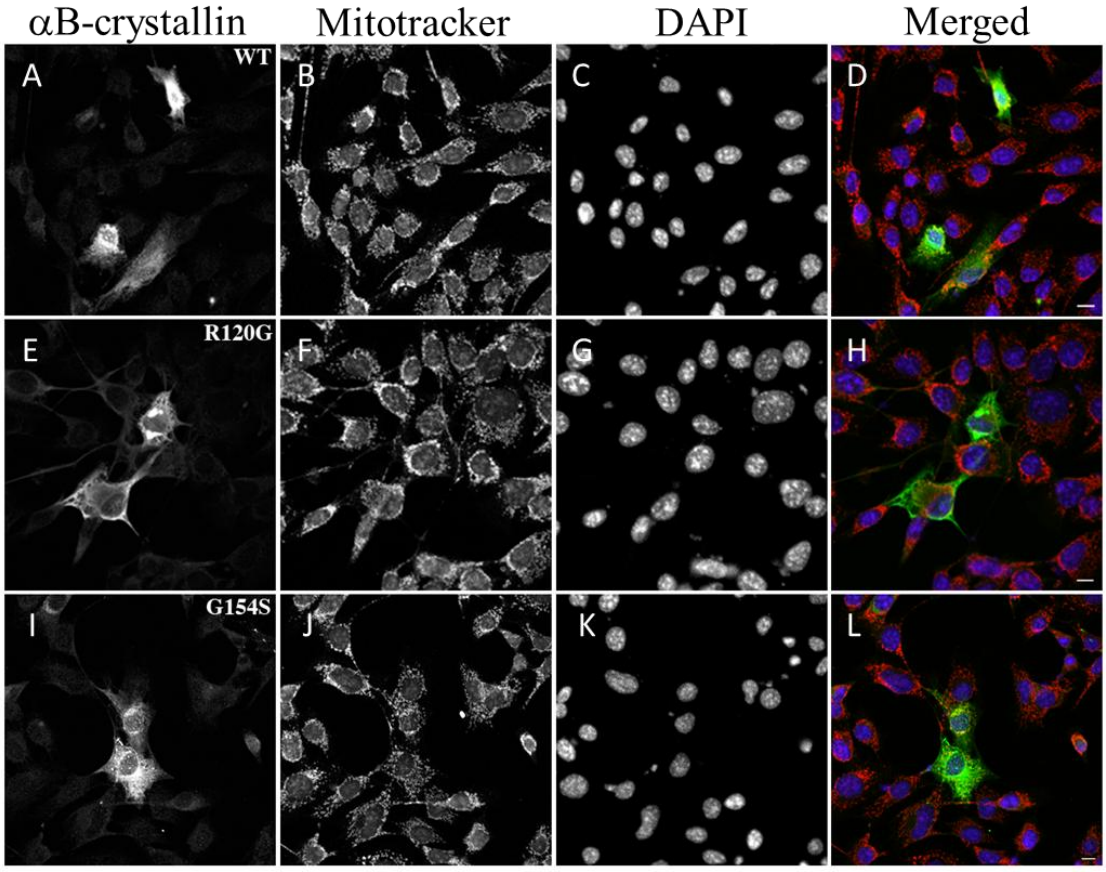

Figure 2-7. Effect of αB-crystallin mutations upon mitochondrial distribution in C2C12 cells. C2C12 cells were tansiently transfected with either wild type or mutant αB-crystallin. At 48 hours after transfection, cells were incubated with MitoTracker® Red CMXRos for 45 minutes at 37℃ to label the mitochondria (B, F, and J). After fixation, cells were counterstained with monoclonal anti-αB-crystallin antibody (A, E, and I). Images were acquired by a confocal laser scanning microscope with αB-crystallin signal in the green channel and mitochondrial signal in the red channel. Merged images show the superimposition of red and green signals with areas overlap appearing yellow (D, H, and L). The nuclei were visualized by counterstaining with DAPI (C, G, and K). Bar, 10 μm.

Figure 2-8. The problems and improvements in co-immunoprecipitation.

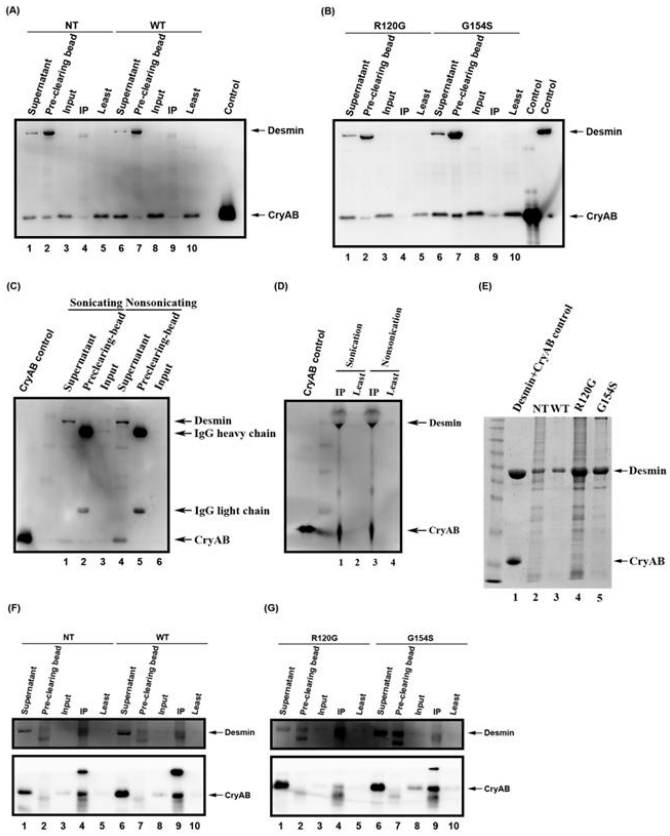

Figure 2-8. The problems and improvements in co-immunoprecipitation. C2C12 transfected with αB-crystallin cells and untransfected C2C12 cells were extracted with triton-X100 buffer and fractionated by centrifuge at 12000rpm for 10 minutes. The resulting of supernatants were applied to Co-IP. The first problem was presence that desmin non-specifically binds to protein G beads in every pre-clearing bead fractions (A and B, lane 2 and 7) at the 2500rpm centrifuge for 3 minutes. Two improvements were concerned that protein G were pre-blocked with 5% BSA in fresh PBS before capturing the antibodies-αB-crystallin complex and supernatants were sonicated before processing Co-IP. The improvements figured out the non-specific binding of desmin to protein G beads (C, lane 2 and 5) in untransfected cells but not in transfected-αB-crystallin cells (F, lane 7 and G, lane 2 and 7). Desmin was captured from protein G-αB-crystallin complex (D, lane 1 and 3) in untransfected cells. To find out this difference, pre-clearing bead fractions were analyzed by SDS-PAGE following coomassie blue staining (E). Desmin in R120G and G154S transfected cells have the lowest solubility (E, lane 2-5). Supernatant, preclearing-bead, input, IP, and least fractions were indicated. Immunoblotting was against monoclonal anti-αB-crystallin antibodies and polyclonal anti-desmin antibodies.

Figure 2-9. Co-immunoprecipitation of NT, WT, R120G, and G154S αB-crystallin in C2C12 cells.

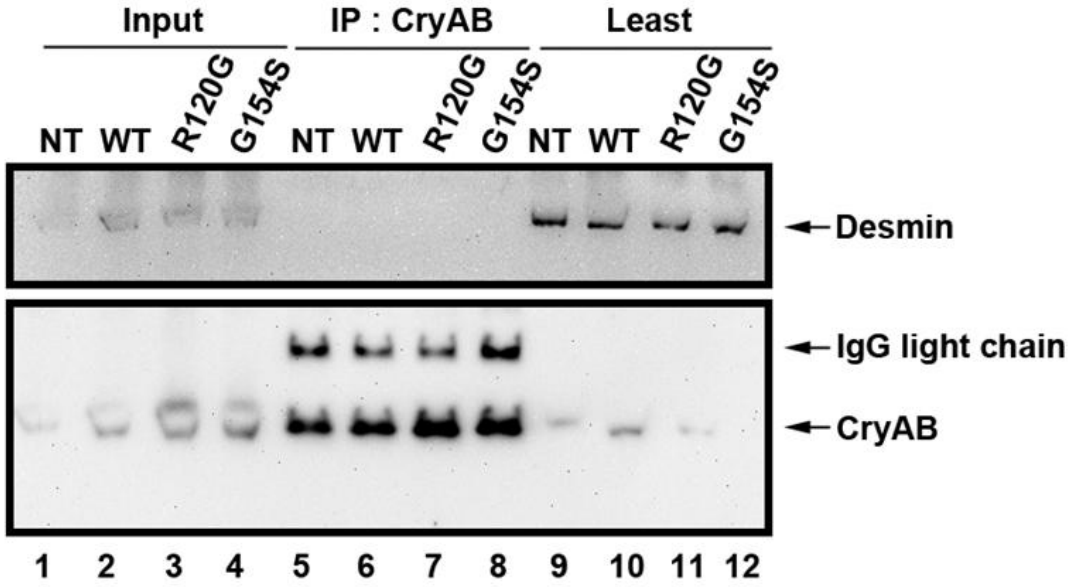

Figure 2-9. Co-immunoprecipitation of NT, WT, R120G, and G154S αB-crystallin in C2C12 cells. At 48 hours posttransfection of αB-crystallin, cells were homogenized in RIPA buffer and fractionated by centrifuge at 12000rpm for 10 minutes. The concentration of resulting supernatants were determined by BCA assay kit. To decrease protein complexity, the protein concentration of supernatants should be dilute into 0.5mg/ml. To prevent self-accumulation of proteins including desmin and increase the soluble desmin in the supernatant, the resulting supernatants were without storing at -20℃ and disolved in RIPA buffer. The input fractions shows that desmin presented in Input fraction initially (Lane 1~4) and almost found in Least fraction (Lane, 9~12). Although monoclonal anti-αB-crystallin antibodies efficiently captured αB-crystallin (Lane 5~8), desmin doesn't bind to αB-crystallin in RIPA buffer.

Figure 3-1. Killing curve of BHK21 cells treated with G418 and hygromycin.

	Day1	day2	day3	day4	day5	day6	day7	day8	Day9	day10	day11	Day12
1-25	+	+	+	+	+	+	+	+	+	+	+	+
1-50	+	+	+	+	+	+	+	+	+	+	+	+
1-100	+	+	+	+	–	–	–	–	–	–	–	–
1-200	+	+	+	–	–	–	–	–	–	–	–	–
1-400	+	+	–	–	–	–	–	–	–	–	–	–
1-800	+	–	–	–	–	–	–	–	–	–	–	–

	Day1	day2	day3	day4	day5	day6	day7	day8	Day9	day10	day11	Day12
2-25	+	+	+	–	–	–	–	–	–	–	–	–
2-50	+	+	+	–	–	–	–	–	–	–	–	–
2-100	+	+	+	–	–	–	–	–	–	–	–	–
2-200	+	+	–	–	–	–	–	–	–	–	–	–
2-400	+	+	–	–	–	–	–	–	–	–	–	–
2-800	+	–	–	–	–	–	–	–	–	–	–	–

Figure 3-1. Killing curve of BHK21 cells treated with G418 and hygromycin. 1-25~1-800 means that BHK21 cells were treated with 400ug/ml G418 and 25~800 ug/ml variants hygromycin and 2-25~2-800 means that BHK21 cells were treated with 1mg/ml G418 and 25~800 ug/ml variants hygromycin. The elucidation of killing curve shows that treating with 1mg/ml of G418 into DMEM was too toxicity so that cells dead in three days. The ideal concentration of both G418 and hygromycin do not more than 500ug/ml as principle.

Figure 3-2. Stable clones were selected from single cell in each 96 well petri dish.

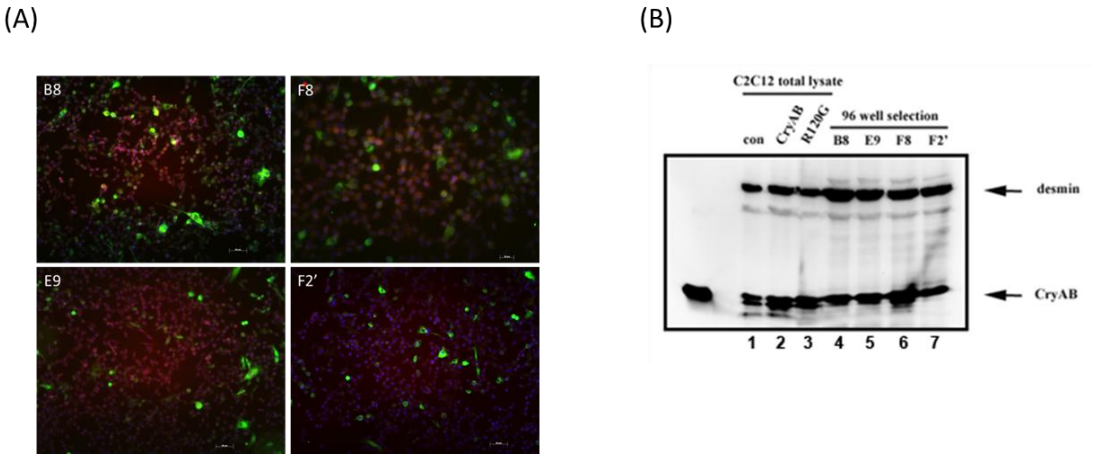

Figure 3-2. Stable clones were selected from single cell in each 96 well petri dish. The distribution of αB-crystallin was labeled with monoclonal anti-αB-crystallin antibodies (A) which is the green channel and DAPI which is the blue channel. Stable clones were cultured to 80% confluence and extracted with triton X-100 buffer and consequent analysis by immunoblotting (B) by probed with monoclonal anti-desmin and anti-αB-crystallin antibodies. To compare the expression level between transiently transfected cells and stable clones, C2C12 transfected with αB-crystallin cells (B, lane 1~3) were analyzed with αB-crystallin stable clones (B, lane 4~7). Desmin and αB-crystallin were pointed by arrows. B8, E9, and F8 was the wild type αB-crystallin stable clones. F2' was the R120G αB-crystallin stable clone. Bar, 50μm.

Figure 3-3. Expression level of αB-crystallin in selected BHK21 stable clones.

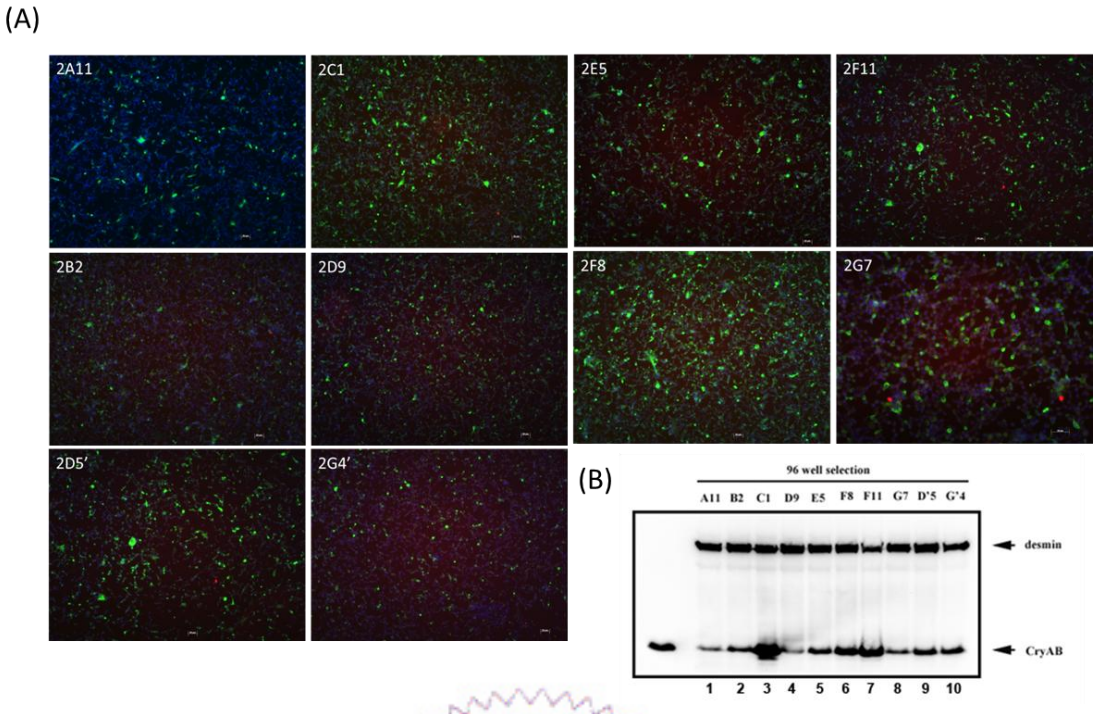

Figure 3-3. Expression level of αB-crystallin in selected BHK21 stable clones. The distribution of αB-crystallin in these selected stable clones were labeled with monoclonal anti-αB-crystallin (A) which is the green channel and DAPI which is the blue channel. When cells grow into 80% confluence, cells extracted with triton X-100 buffer and consequent analysis by immunoblotting (B) by probed with monoclonal anti-desmin and anti-αB-crystallin antibodies. The 2C1 clone significantly expressed most αB-crystallin, but no one express the same amounts of R120G αB-crystallin. 2E5 and 2G4' were expressed equal amounts of αB-crystallin that were applied to cytoskeletal preparation (Fig. 3.4). These stable clone included 2A11, 2B2, 2C1, 2D9, 2E5, 2F8, 2F11, and 2G7 were wild type αB-crystallin stable clones. 2D5' and 2G4' were R120G αB-crystallin stable clones. Bar, 50 μm.

Figure 3-4. Cytoskeletal preparation was analyzed by coomassie blue staining and silver staining.

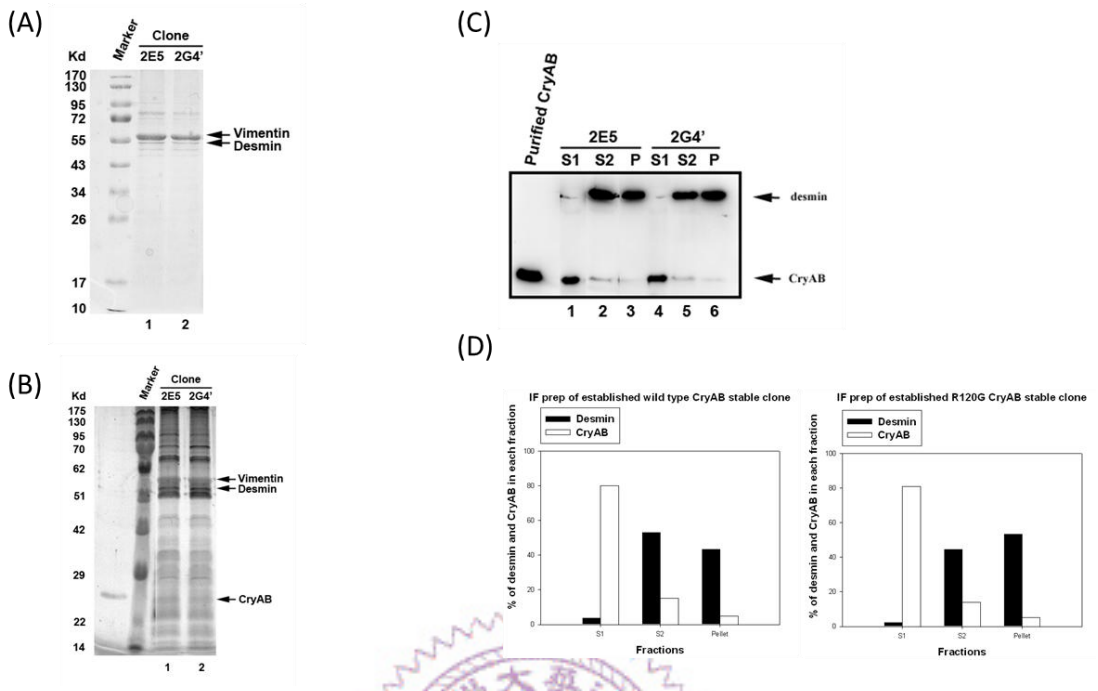

Figure 3-4. Cytoskeletal preparation was analyzed by coomassie blue staining and silver staining. 2E5 and 2G4' clones expressed approximately amounts of αB-crystallin according to immunoblotting (Figure 3.3). The distribution of intracellular proteins was analyzed by SDS-PAGE following either coomassie blue (A) staining or silver staining (B) in 2E5 and 2G4' stable clones. The molecular size of vimentin, desmin, and αB-crystallin were indicated by arrows. The evidence shows that vimentin intermediate filament was the major protein in the C2C12 cell. Triton-soluble intracellular molecular was released in S1 (Supernatant 1). Cytoskeletal proteins were released by dissolved with high salt buffer containing 1.5 M KCl. Desmin in 2E5 clone was more soluble than in 2G4' clone (D). And R120G αB-crystallin in stable clone becomes more triton-soluble (C, lane 4) in contrast to cell fraction study.

Figure 3-5. Expression level of R120G αB-crystallin stable clones.

(A)

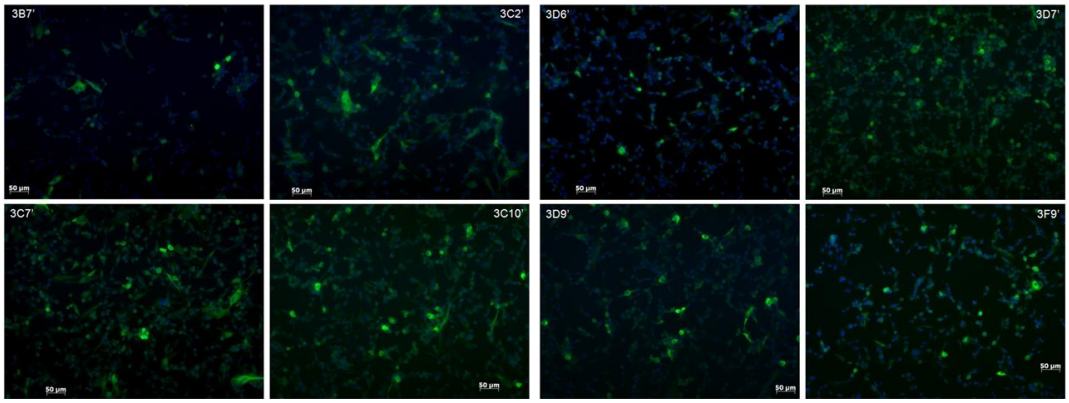

(B)

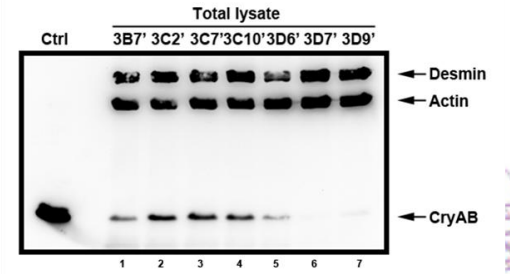

Figure 3-5. Expression level of R120G αB-crystallin stable clones. The expression level of αB-crystallin in these selected stable clones were labeled with monoclonal anti-αB-crystallin (A) which is the green channel and DAPI which is the blue channel. Cells were then analized by western blotting (B). These clones expressed low levels of R120G αB-crystallin. These R120 G αB-crystallin stable clones included 3B7', 3C2', 3C7', 3C10', 3D6', 3D7', 3D9', and 3F9' were indicated. Bar, 50μm.

Figure 3-6. R120G αB-crystallin was examined by immunofluorecent microscopy.

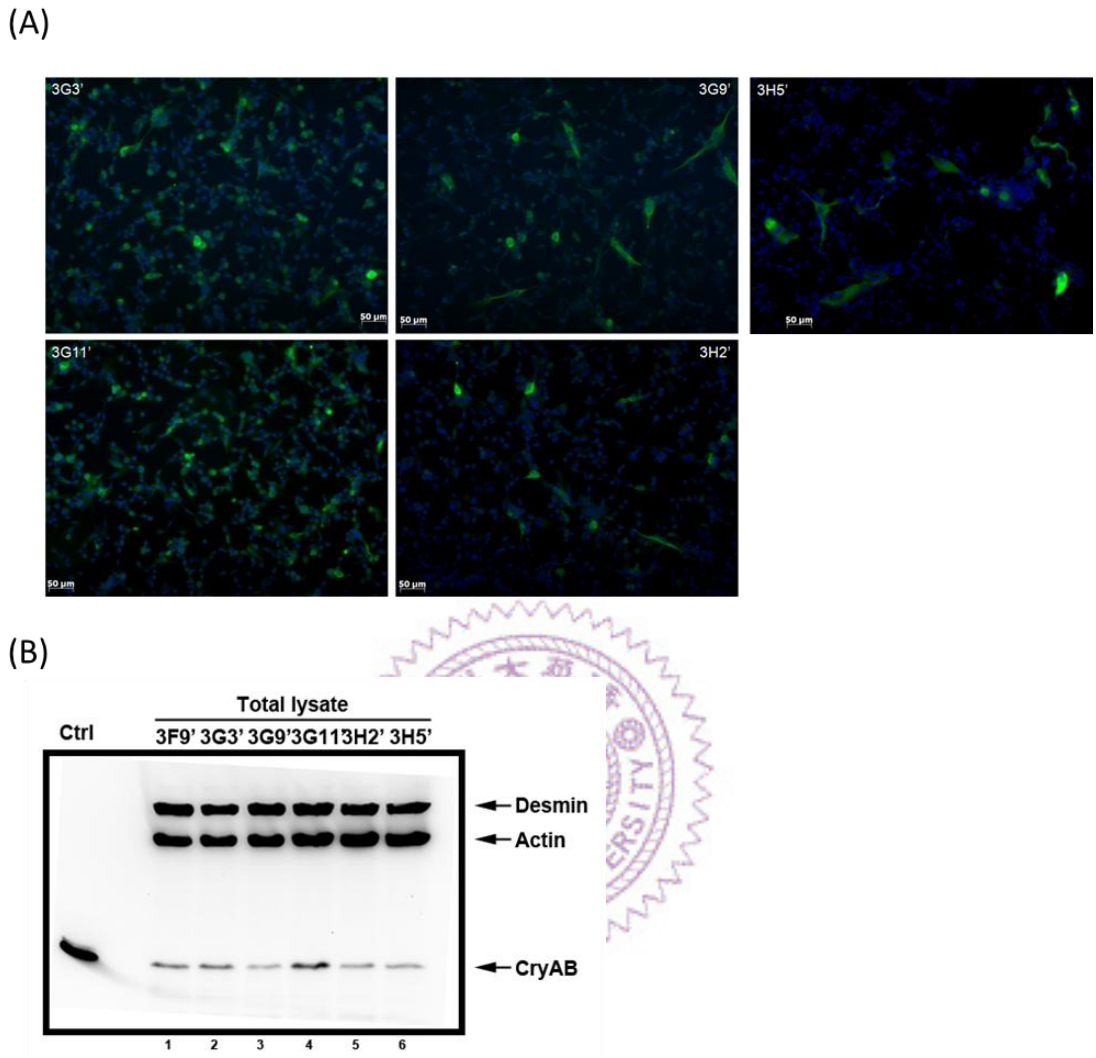

Figure 3-6. R120G αB-crystallin was examined by immunofluorecent microscopy. αB-crystallin was labeled against monoclonal anti-αB-crystallin antibodies, which shows in green channel and DAPI, which shows in blue channel. αB-crystallin expression was indicated according to immunoblotting. These stable clones also express low levels amounts of R120G αB-crystallin. These stable clone included 3F9', 3G3', 3G9', 3G11', 3H2', and 3H5' were indicated. Bar, 50μm.

Figure 3-7. C2C12 stable clone selection of cells expressed transfected αB-crystallin.

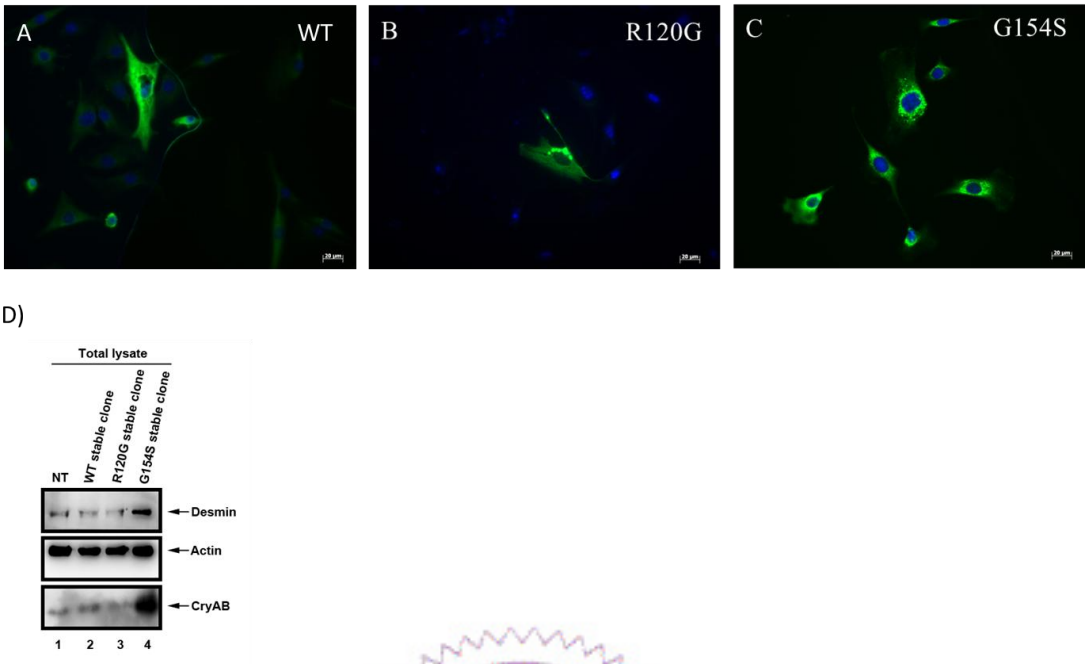

Figure 3-7. C2C12 stable clone selection of cells expressed transfected αB-crystallin. These αB-crystallin stable clones were selected by treating 0.4 mg/ml G418 and 0.2mg/ml hygromycine for approximately two weeks. When cells grew into 80% confluence, cells were fixed and counterstained both with monoclonal αB-crystallin antibodies, which is the green channel, and DAPI, which is the blue channel. The images show that the expression level of αB-crystallin selection was not vary efficient and the effect that causing by stable transfected αB-crystallin. The distribution of wild type αB-crystallin (A) was throughout the cell, in contrast, R120G αB-crystallin (B) formed cytoplasmic aggresomes perinuclear. G154S αB-crystallin (C) highly express insight the individual cell and tend to close to nuclear although absence of aggresomes. After stable transfection with αB-crystallin, cells were collected and lysed when cells grew into 80% confluences. The fractionation condition was the same with studies of transiently transfection. In contrast to no transfected cells (D, lane1), the efficiency of drag selection was not good enough. Bar, 20μm.

References

[1] D.A. Parry, P.M. Steinert, Intermediate filaments: molecular architecture, assembly, dynamics and polymorphism, Q Rev Biophys 32 (1999) 99-187.

[2] H. Herrmann, U. Aebi, Intermediate filaments: molecular structure, assembly mechanism, and integration into functionally distinct intracellular Scaffolds, Annu Rev Biochem 73 (2004) 749-789.

[3] A. Zimek, R. Stick, K. Weber, Genes coding for intermediate filament proteins: common features and unexpected differences in the genomes of humans and the teleost fish Fugu rubripes, J Cell Sci 116 (2003) 2295-2302.

[4] M. Hesse, T.M. Magin, K. Weber, Genes for intermediate filament proteins and the draft sequence of the human genome: novel keratin genes and a surprisingly high number of pseudogenes related to keratin genes 8 and 18, J Cell Sci 114 (2001) 2569-2575.

[5] D.A. Parry, Microdissection of the sequence and structure of intermediate filament chains, Adv Protein Chem 70 (2005) 113-142.

[6] D.A. Parry, S.V. Strelkov, P. Burkhard, U. Aebi, H. Herrmann, Towards a molecular description of intermediate filament structure and assembly, Exp Cell Res 313 (2007) 2204-2216.

[7] H. Herrmann, M. Haner, M. Brettel, N.O. Ku, U. Aebi, Characterization of distinct early assembly units of different intermediate filament proteins, J Mol Biol 286 (1999) 1403-1420.

[8] V. Prahlad, M. Yoon, R.D. Moir, R.D. Vale, R.D. Goldman, Rapid movements of vimentin on microtubule tracks: kinesin-dependent assembly of intermediate filament networks, J Cell Biol 143 (1998) 159-170.

[9] M. Yoon, R.D. Moir, V. Prahlad, R.D. Goldman, Motile properties of vimentin intermediate filament networks in living cells, J Cell Biol 143 (1998) 147-157.

[10] K.L. Vikstrom, G.G. Borisy, R.D. Goldman, Dynamic aspects of intermediate filament networks in BHK-21 cells, Proc Natl Acad Sci U S A 86 (1989) 549-553.

[11] M.B. Omary, P.A. Coulombe, W.H. McLean, Intermediate filament proteins and their associated diseases, N Engl J Med 351 (2004) 2087-2100.

[12] L.M. Godsel, R.P. Hobbs, K.J. Green, Intermediate filament assembly: dynamics to disease, Trends Cell Biol 18 (2008) 28-37.

[13] P.A. Coulombe, M.L. Kerns, E. Fuchs, Epidermolysis bullosa simplex: a paradigm for disorders of tissue fragility, J Clin Invest 119 (2009) 1784-1793.

[14] Z. Li, P. Marchand, J. Humbert, C. Babinet, D. Paulin, Desmin sequence elements regulating skeletal muscle-specific expression in transgenic mice,

Development 117 (1993) 947-959.

[15] D.O. Furst, M. Osborn, K. Weber, Myogenesis in the mouse embryo: differential onset of expression of myogenic proteins and the involvement of titin in myofibril assembly, J Cell Biol 109 (1989) 517-527.

[16] G. Schaart, C. Viebahn, W. Langmann, F. Ramaekers, Desmin and titin expression in early postimplantation mouse embryos, Development 107 (1989) 585-596.

[17] D.L. Gard, E. Lazarides, The synthesis and distribution of desmin and vimentin during myogenesis in vitro, Cell 19 (1980) 263-275.

[18] P.M. Hemken, R.M. Bellin, S.W. Sernett, B. Becker, T.W. Huiatt, R.M. Robson, Molecular characteristics of the novel intermediate filament protein paranemin. Sequence reveals EAP-300 and IFAPa-400 are highly homologous to paranemin, J Biol Chem 272 (1997) 32489-32499.

[19] S.C. Schweitzer, M.W. Klymkowsky, R.M. Bellin, R.M. Robson, Y. Capetanaki, R.M. Evans, Paranemin and the organization of desmin filament networks, J Cell Sci 114 (2001) 1079-1089.

[20] M.G. Price, E. Lazarides, Expression of intermediate filament-associated proteins paranemin and synemin in chicken development, J Cell Biol 97 (1983) 1860-1874.

[21] E. Poon, E.V. Howman, S.E. Newey, K.E. Davies, Association of syncoilin and desmin: linking intermediate filament proteins to the dystrophin-associated protein complex, J Biol Chem 277 (2002) 3433-3439.

[22] Y. Mizuno, T.G. Thompson, J.R. Guyon, H.G. Lidov, M. Brosius, M. Imamura, E. Ozawa, S.C. Watkins, L.M. Kunkel, Desmuslin, an intermediate filament protein that interacts with alpha -dystrobrevin and desmin, Proc Natl Acad Sci U S A 98 (2001) 6156-6161.

[23] T. Hijikata, T. Murakami, M. Imamura, N. Fujimaki, H. Ishikawa, Plectin is a linker of intermediate filaments to Z-discs in skeletal muscle fibers, J Cell Sci 112 (Pt 6) (1999) 867-876.

[24] R. Schroder, I. Warlo, H. Herrmann, P.F. van der Ven, C. Klasen, I. Blumcke, R.R. Mundegar, D.O. Furst, H.H. Goebel, T.M. Magin, Immunogold EM reveals a close association of plectin and the desmin cytoskeleton in human skeletal muscle, Eur J Cell Biol 78 (1999) 288-295.

[25] M.G. Price, Molecular analysis of intermediate filament cytoskeleton--a putative load-bearing structure, Am J Physiol 246 (1984) H566-572.

[26] E. Viegas-Pequignot, Z.L. Li, B. Dutrillaux, F. Apiou, D. Paulin, Assignment of human desmin gene to band 2q35 by nonradioactive in situ hybridization, Hum Genet 83 (1989) 33-36.

[27] Z.L. Li, A. Lilienbaum, G. Butler-Browne, D. Paulin, Human desmin-coding gene: complete nucleotide sequence, characterization and regulation of expression during myogenesis and development, Gene 78 (1989) 243-254.

[28] K. Weber, N. Geisler, Intermediate filaments: structural conservation and divergence, Ann N Y Acad Sci 455 (1985) 126-143.

[29] S.V. Strelkov, H. Herrmann, U. Aebi, Molecular architecture of intermediate filaments, Bioessays 25 (2003) 243-251.

[30] L.G. Goldfarb, M.C. Dalakas, Tragedy in a heartbeat: malfunctioning desmin causes skeletal and cardiac muscle disease, J Clin Invest 119 (2009) 1806-1813.

[31] R.P. Taylor, I.J. Benjamin, Small heat shock proteins: a new classification scheme in mammals, J Mol Cell Cardiol 38 (2005) 433-444.

[32] R.A. Dubin, A.H. Ally, S. Chung, J. Piatigorsky, Human alphaB-crystallin gene and preferential promoter function in lens, Genomics 7 (1990) 594-601.

[33] J. Horwitz, The function of alpha-crystallin in vision, Semin Cell Dev Biol 11 (2000) 53-60.

[34] W.C. Boelens, Y. Croes, W.W. de Jong, Interaction between alphaB-crystallin and the human 20S proteasomal subunit C8/alpha7, Biochim Biophys Acta 1544 (2001) 311-319.

[35] J. den Engelsman, V. Keijsers, W.W. de Jong, W.C. Boelens, The small heat-shock protein alpha αB-crystallin promotes FBX4-dependent ubiquitination, J Biol Chem 278 (2003) 4699-4704.

[36] A.P. Arrigo, The cellular "networking" of mammalian Hsp27 and its functions in the control of protein folding, redox state and apoptosis, Adv Exp Med Biol 594 (2007) 14-26.

[37] M.C. Kamradt, F. Chen, V.L. Cryns, The small heat shock protein alpha B-crystallin negatively regulates cytochrome c- and caspase-8-dependent activation of caspase-3 by inhibiting its autoproteolytic maturation, J Biol Chem 276 (2001) 16059-16063.

[38] Y.W. Mao, J.P. Liu, H. Xiang, D.W. Li, Human alphaA- and alphaB-crystallins bind to Bax and Bcl-X(S) to sequester their translocation during staurosporine-induced apoptosis, Cell Death Differ 11 (2004) 512-526.

[39] D.W. Li, J.P. Liu, Y.W. Mao, H. Xiang, J. Wang, W.Y. Ma, Z. Dong, H.M. Pike, R.E. Brown, J.C. Reed, Calcium-activated RAF/MEK/ERK signaling pathway mediates p53-dependent apoptosis and is abrogated by alphaB-crystallin through inhibition of RAS activation, Mol Biol Cell 16 (2005) 4437-4453.

[40] K. Wang, A. Spector, alpha-crystallin stabilizes actin filaments and prevents cytochalasin-induced depolymerization in a phosphorylation-dependent

manner, Eur J Biochem 242 (1996) 56-66.

[41] M. Wieske, R. Benndorf, J. Behlke, R. Dolling, G. Grelle, H. Bielka, G. Lutsch, Defined sequence segments of the small heat shock proteins HSP25 and alphaB-crystallin inhibit actin polymerization, Eur J Biochem 268 (2001) 2083-2090.

[42] B.N. Singh, K.S. Rao, T. Ramakrishna, N. Rangaraj, M. Rao Ch, Association of alphaB-crystallin, a small heat shock protein, with actin: role in modulating actin filament dynamics in vivo, J Mol Biol 366 (2007) 756-767.

[43] T. Iwaki, A. Iwaki, J. Tateishi, J.E. Goldman, Sense and antisense modification of glial alphaB-crystallin production results in alterations of stress fiber formation and thermoresistance, J Cell Biol 125 (1994) 1385-1393.

[44] J.G. Ghosh, S.A. Houck, J.I. Clark, Interactive sequences in the stress protein and molecular chaperone human alphaB crystallin recognize and modulate the assembly of filaments, Int J Biochem Cell Biol 39 (2007) 1804-1815.

[45] Y. Fujita, E. Ohto, E. Katayama, Y. Atomi, alphaB-Crystallin-coated MAP microtubule resists nocodazole and calcium-induced disassembly, J Cell Sci 117 (2004) 1719-1726.

[46] E. Ohto-Fujita, Y. Fujita, Y. Atomi, Analysis of the alphaB-crystallin domain responsible for inhibiting tubulin aggregation, Cell Stress Chaperones 12 (2007) 163-171.

[47] J.G. Ghosh, S.A. Houck, J.I. Clark, Interactive domains in the molecular chaperone human alphaB crystallin modulate microtubule assembly and disassembly, PLoS One 2 (2007) e498.

[48] I.D. Nicholl, R.A. Quinlan, Chaperone activity of alpha-crystallins modulates intermediate filament assembly, EMBO J 13 (1994) 945-953.

[49] P.J. Muchowski, M.M. Valdez, J.I. Clark, AlphaB-crystallin selectively targets intermediate filament proteins during thermal stress, Invest Ophthalmol Vis Sci 40 (1999) 951-958.

[50] K. Djabali, B. de Nechaud, F. Landon, M.M. Portier, AlphaB-crystallin interacts with intermediate filaments in response to stress, J Cell Sci 110 (Pt 21) (1997) 2759-2769.

[51] M.D. Perng, L. Cairns, I.P. van den, A. Prescott, A.M. Hutcheson, R.A. Quinlan, Intermediate filament interactions can be altered by HSP27 and alphaB-crystallin, J Cell Sci 112 (Pt 13) (1999) 2099-2112.

[52] T. Wisniewski, J.E. Goldman, Alpha B-crystallin is associated with intermediate filaments in astrocytoma cells, Neurochem Res 23 (1998) 385-392.

[53] M.D. Perng, S.F. Wen, I.P. van den, A.R. Prescott, R.A. Quinlan, Desmin

aggregate formation by R120G alphaB-crystallin is caused by altered filament interactions and is dependent upon network status in cells, Mol Biol Cell 15 (2004) 2335-2346.

[54] M.D. Perng, P.J. Muchowski, I.P. van Den, G.J. Wu, A.M. Hutcheson, J.I. Clark, R.A. Quinlan, The cardiomyopathy and lens cataract mutation in alphaB-crystallin alters its protein structure, chaperone activity, and interaction with intermediate filaments in vitro, J Biol Chem 274 (1999) 33235-33243.

[55] F. Bennardini, A. Wrzosek, M. Chiesi, Alpha B-crystallin in cardiac tissue. Association with actin and desmin filaments, Circ Res 71 (1992) 288-294.

[56] P. Vicart, A. Caron, P. Guicheney, Z. Li, M.C. Prevost, A. Faure, D. Chateau, F. Chapon, F. Tome, J.M. Dupret, D. Paulin, M. Fardeau, A missense mutation in the alphaB-crystallin chaperone gene causes a desmin-related myopathy, Nat Genet 20 (1998) 92-95.

[57] L.G. Goldfarb, P. Vicart, H.H. Goebel, M.C. Dalakas, Desmin myopathy, Brain 127 (2004) 723-734.

[58] J. Lowe, A. Blanchard, K. Morrell, G. Lennox, L. Reynolds, M. Billett, M. Landon, R.J. Mayer, Ubiquitin is a common factor in intermediate filament inclusion bodies of diverse type in man, including those of Parkinson's disease, Pick's disease, and Alzheimer's disease, as well as Rosenthal fibres in cerebellar astrocytomas, cytoplasmic bodies in muscle, and mallory bodies in alcoholic liver disease, J Pathol 155 (1988) 9-15.

[59] M.A. Pappolla, Lewy bodies of Parkinson's disease. Immune electron microscopic demonstration of neurofilament antigens in constituent filaments, Arch Pathol Lab Med 110 (1986) 1160-1163.

[60] R.A. Quinlan, M. Brenner, J.E. Goldman, A. Messing, GFAP and its role in Alexander disease, Exp Cell Res 313 (2007) 2077-2087.

[61] K. Zatloukal, S.W. French, C. Stumptner, P. Strnad, M. Harada, D.M. Toivola, M. Cadrin, M.B. Omary, From Mallory to Mallory-Denk bodies: what, how and why?, Exp Cell Res 313 (2007) 2033-2049.

[62] R. Quinlan, P. Van Den Ijssel, Fatal attraction: when chaperone turns harlot, Nat Med 5 (1999) 25-26.

[63] L.G. Goldfarb, K.Y. Park, L. Cervenakova, S. Gorokhova, H.S. Lee, O. Vasconcelos, J.W. Nagle, C. Semino-Mora, K. Sivakumar, M.C. Dalakas, Missense mutations in desmin associated with familial cardiac and skeletal myopathy, Nat Genet 19 (1998) 402-403.

[64] M. Fardeau, P. Vicart, A. Caron, D. Chateau, M. Chevallay, H. Collin, F. Chapon, D. Duboc, B. Eymard, F.M. Tome, J.M. Dupret, D. Paulin, P. Guicheney, [Familial myopathy with desmin storage seen as a

granulo-filamentar, electron-dense material with mutation of the alphaB-cristallin gene], Rev Neurol (Paris) 156 (2000) 497-504.

[65] M.P. Bova, O. Yaron, Q. Huang, L. Ding, D.A. Haley, P.L. Stewart, J. Horwitz, Mutation R120G in alphaB-crystallin, which is linked to a desmin-related myopathy, results in an irregular structure and defective chaperone-like function, Proc Natl Acad Sci U S A 96 (1999) 6137-6142.

[66] A.T. Chavez Zobel, A. Loranger, N. Marceau, J.R. Theriault, H. Lambert, J. Landry, Distinct chaperone mechanisms can delay the formation of aggresomes by the myopathy-causing R120G alphaB-crystallin mutant, Hum Mol Genet 12 (2003) 1609-1620.

[67] L. Fu, J.J. Liang, Alteration of protein-protein interactions of congenital cataract crystallin mutants, Invest Ophthalmol Vis Sci 44 (2003) 1155-1159.

[68] X. Wang, H. Osinska, R. Klevitsky, A.M. Gerdes, M. Nieman, J. Lorenz, T. Hewett, J. Robbins, Expression of R120G-alphaB-crystallin causes aberrant desmin and alphaB-crystallin aggregation and cardiomyopathy in mice, Circ Res 89 (2001) 84-91.

[69] V. Berry, P. Francis, M.A. Reddy, D. Collyer, E. Vithana, I. MacKay, G. Dawson, A.H. Carey, A. Moore, S.S. Bhattacharya, R.A. Quinlan, Alpha-B crystallin gene (CRYAB) mutation causes dominant congenital posterior polar cataract in humans, Am J Hum Genet 69 (2001) 1141-1145.

[70] D. Selcen, A.G. Engel, Myofibrillar myopathy caused by novel dominant negative alpha B-crystallin mutations, Ann Neurol 54 (2003) 804-810.

[71] N. Inagaki, T. Hayashi, T. Arimura, Y. Koga, M. Takahashi, H. Shibata, K. Teraoka, T. Chikamori, A. Yamashina, A. Kimura, Alpha B-crystallin mutation in dilated cardiomyopathy, Biochem Biophys Res Commun 342 (2006) 379-386.

[72] P. Reilich, B. Schoser, N. Schramm, S. Krause, J. Schessl, W. Kress, J. Muller-Hocker, M.C. Walter, H. Lochmuller, The p.G154S mutation of the alpha-B crystallin gene (CRYAB) causes late-onset distal myopathy, Neuromuscul Disord 20 (2010) 255-259.

[73] H. Bar, N. Mucke, A. Kostareva, G. Sjoberg, U. Aebi, H. Herrmann, Severe muscle disease-causing desmin mutations interfere with in vitro filament assembly at distinct stages, Proc Natl Acad Sci U S A 102 (2005) 15099-15104.

[74] H. Bar, A. Kostareva, G. Sjoberg, T. Sejersen, H.A. Katus, H. Herrmann, Forced expression of desmin and desmin mutants in cultured cells: impact of myopathic missense mutations in the central coiled-coil domain on network formation, Exp Cell Res 312 (2006) 1554-1565.

[75] H. Bar, N. Mucke, P. Ringler, S.A. Muller, L. Kreplak, H.A. Katus, U. Aebi, H. Herrmann, Impact of disease mutations on the desmin filament assembly process, J Mol Biol 360 (2006) 1031-1042.

[76] H. Bar, N. Mucke, H.A. Katus, U. Aebi, H. Herrmann, Assembly defects of desmin disease mutants carrying deletions in the alpha-helical rod domain are rescued by wild type protein, J Struct Biol 158 (2007) 107-115.

[77] H. Bar, B. Goudeau, S. Walde, M. Casteras-Simon, N. Mucke, A. Shatunov, Y.P. Goldberg, C. Clarke, J.L. Holton, B. Eymard, H.A. Katus, M. Fardeau, L. Goldfarb, P. Vicart, H. Herrmann, Conspicuous involvement of desmin tail mutations in diverse cardiac and skeletal myopathies, Hum Mutat 28 (2007) 374-386.

[78] Y. Capetanaki, R.J. Bloch, A. Kouloumenta, M. Mavroidis, S. Psarras, Muscle intermediate filaments and their links to membranes and membranous organelles, Exp Cell Res 313 (2007) 2063-2076.

[79] X. Wang, H. Osinska, G.W. Dorn, 2nd, M. Nieman, J.N. Lorenz, A.M. Gerdes, S. Witt, T. Kimball, J. Gulick, J. Robbins, Mouse model of desmin-related cardiomyopathy, Circulation 103 (2001) 2402-2407.

[80] A. Kostareva, G. Sjoberg, J. Bruton, S.J. Zhang, J. Balogh, A. Gudkova, B. Hedberg, L. Edstrom, H. Westerblad, T. Sejersen, Mice expressing L345P mutant desmin exhibit morphological and functional changes of skeletal and cardiac mitochondria, J Muscle Res Cell Motil 29 (2008) 25-36.

[81] A. Maloyan, A. Sanbe, H. Osinska, M. Westfall, D. Robinson, K. Imahashi, E. Murphy, J. Robbins, Mitochondrial dysfunction and apoptosis underlie the pathogenic process in alpha-B-crystallin desmin-related cardiomyopathy, Circulation 112 (2005) 3451-3461.

[82] N.S. Rajasekaran, P. Connell, E.S. Christians, L.J. Yan, R.P. Taylor, A. Orosz, X.Q. Zhang, T.J. Stevenson, R.M. Peshock, J.A. Leopold, W.H. Barry, J. Loscalzo, S.J. Odelberg, I.J. Benjamin, Human alpha B-crystallin mutation causes oxido-reductive stress and protein aggregation cardiomyopathy in mice, Cell 130 (2007) 427-439.

[83] U.P. Andley, P.D. Hamilton, N. Ravi, C.C. Weihl, A knock-in mouse model for the R120G mutation of alphaB-crystallin recapitulates human hereditary myopathy and cataracts, PLoS One 6 (2011) e17671.

[84] M. Li, M.C. Dalakas, Abnormal desmin protein in myofibrillar myopathies caused by desmin gene mutations, Ann Neurol 49 (2001) 532-536.

[85] R.R. Kopito, Aggresomes, inclusion bodies and protein aggregation, Trends Cell Biol 10 (2000) 524-530.

[86] A. Sanbe, H. Osinska, J.E. Saffitz, C.G. Glabe, R. Kayed, A. Maloyan, J.

Robbins, Desmin-related cardiomyopathy in transgenic mice: a cardiac amyloidosis, Proc Natl Acad Sci U S A 101 (2004) 10132-10136.

[87] H. Ecroyd, J.A. Carver, Crystallin proteins and amyloid fibrils, Cell Mol Life Sci 66 (2009) 62-81.

[88] J.D. Lunemann, J. Schmidt, D. Schmid, K. Barthel, A. Wrede, M.C. Dalakas, C. Munz, Beta-amyloid is a substrate of autophagy in sporadic inclusion body myositis, Ann Neurol 61 (2007) 476-483.

[89] P. Tannous, H. Zhu, J.L. Johnstone, J.M. Shelton, N.S. Rajasekaran, I.J. Benjamin, L. Nguyen, R.D. Gerard, B. Levine, B.A. Rothermel, J.A. Hill, Autophagy is an adaptive response in desmin-related cardiomyopathy, Proc Natl Acad Sci U S A 105 (2008) 9745-9750.

[90] A. Maloyan, J. Robbins, Autophagy in desmin-related cardiomyopathy: Thoughts at the halfway point, Autophagy 6 (2010).

[91] J.S. Pattison, J. Robbins, Autophagy and proteotoxicity in cardiomyocytes, Autophagy 7 (2011).

[92] S. Sarkar, D.C. Rubinsztein, Small molecule enhancers of autophagy for neurodegenerative diseases, Mol Biosyst 4 (2008) 895-901.

[93] S. Sarkar, D.C. Rubinsztein, Huntington's disease: degradation of mutant huntingtin by autophagy, FEBS J 275 (2008) 4263-4270.

[94] The Alexander disease-causing glial fibrillary acidic protein mutant, R416W, accumulates into Rosenthal fibers by a pathway that involves filament aggregation and the association of alpha B-crystallin and HSP27,Am J Hum Genet(2006)79(2):197-213.

[95] Intermediate filament protein structure determination.,Methods Cell Biol (2004) 78:25-43.

[96] A set of anti-crystallin monoclonal antibodies for detecting lens specificities: beta-crystallin as a specific marker for detecting lentoidogenesis in cultures of chicken lens epithelial cells, Jpn J Ophthalmol (1993) 37(4):355-68.

[97] M.D. Perng, A. Sandilands, J. Kuszak, R. Dahm, A. Wegener, A.R. Prescott, R.A. Quinlan, The intermediate filament systems in the eye lens, Methods Cell Biol 78 (2004) 597-624.

[98] S. Simon, M. Michiel, F. Skouri-Panet, J.P. Lechaire, P. Vicart, A. Tardieu, Residue R120 is essential for the quaternary structure and functional integrity of human alphaB-crystallin, Biochemistry 46 (2007) 9605-9614.

[99] S. Meehan, T.P. Knowles, A.J. Baldwin, J.F. Smith, A.M. Squires, P. Clements, T.M. Treweek, H. Ecroyd, G.G. Tartaglia, M. Vendruscolo, C.E. Macphee, C.M. Dobson, J.A. Carver, Characterisation of amyloid fibril formation by small heat-shock chaperone proteins human alphaA-, alphaB- and R120G

alphaB-crystallins, J Mol Biol 372 (2007) 470-484.

[100] L.V. Kumar, T. Ramakrishna, C.M. Rao, Structural and functional consequences of the mutation of a conserved arginine residue in alphaA and alphaB crystallins, J Biol Chem 274 (1999) 24137-24141.

[101] W.W. de Jong, A. Zweers, M. Versteeg, E.C. Nuy-Terwindt, Primary structures of the alpha-crystallin A chains of twenty-eight mammalian species, chicken and frog, Eur J Biochem 141 (1984) 131-140.